JACS Au
AN OPEN ACCESS JOURNAL OF THE AMERICAN CHEMICAL SOCIETY

pubs.acs.org/jacsau
Perspective

Mechanistic Implications of Low CO Coverage on Cu in the Electrochemical CO and CO_2 Reduction Reactions

Xiaoxia Chang, Haocheng Xiong, Qi Lu, and Bingjun Xu*

Cite This: *JACS Au* 2023, 3, 2948−2963

Read Online

ACCESS | Metrics & More | Article Recommendations

ABSTRACT: Electrochemical CO or CO_2 reduction reactions ($CO_{(2)}RR$), powered by renewable energy, represent one of the promising strategies for upgrading CO_2 to valuable products. To design efficient and selective catalysts for the $CO_{(2)}RR$, a comprehensive mechanistic understanding is necessary, including a comprehensive understanding of the reaction network and the identity of kinetically relevant steps. Surface-adsorbed CO (CO_{ad}) is the most commonly reported reaction intermediate in the $CO_{(2)}RR$, and its surface coverage (θ_{CO}) and binding energy are proposed to be key to the catalytic performance. Recent experimental evidence suggests that θ_{CO} on Cu electrode at electrochemical conditions is quite low (~0.05 monolayer), while relatively high θ_{CO} is often assumed in literature mechanistic discussion. This Perspective briefly summarizes existing efforts in determining θ_{CO} on Cu surfaces, analyzes mechanistic impacts of low θ_{CO} on the reaction pathway and catalytic performance, and discusses potential fruitful future directions in advancing our understanding of the Cu-catalyzed $CO_{(2)}RR$.

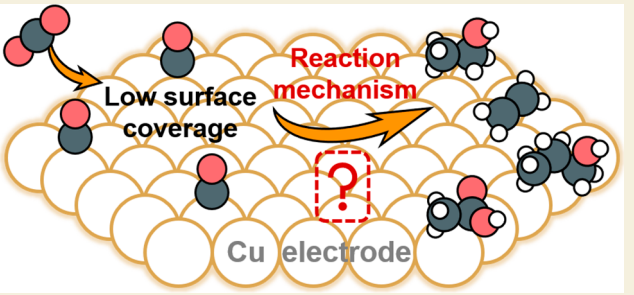

KEYWORDS: *Absolute CO coverage, Cu electrode, CO and CO_2 reduction mechanism, multicarbon products, rate-determining step, reaction order*

1. INTRODUCTION

Renewable-energy-powered CO or CO_2 electroreduction reactions (collectively referred to as the $CO_{(2)}RR$) have been widely recognized as a promising strategy to enable a sustainable carbon cycle.[1−5] Pioneering works by Hori and co-workers four decades ago showed that electrocatalytically active elements can be categorized into four general groups based on their product distribution in the $CO_{(2)}RR$, i.e., selectivity toward H_2, CO, formate and hydrocarbon/oxygenates.[6,7] Cu stands out as the only element capable of converting CO or CO_2 into multicarbon (C_{2+}) products, e.g., ethylene, ethanol, acetate and 1-propanol, with decent selectivities.[8−10] While much effort has been devoted to developing Cu-based electrocatalysts with low overpotential and high selectivity toward one or a few specific products,[3,11] selectivity control remains challenging.[1,3] Effective catalyst design requires detailed knowledge of the reaction mechanism, including reaction network, identity of kinetically relevant steps and key reaction intermediates.[12−18] One of the few aspects in the CO_2RR field with a general consensus is that CO is a necessary intermediate in the formation of C_{2+} products on Cu,[3] as surface adsorbed CO (CO_{ad}) could be readily observed in the CO_2RR on Cu via surface-enhanced vibrational spectroscopies, including infrared (IR) and Raman spectroscopies.[15,19,20] Another key piece of evidence is that the reduction of CO on Cu could lead to a similar C_{2+} product distribution as the CO_2RR under identical conditions.[8] Computational investigations suggested that the CO binding energy to the catalyst surface could serve as a descriptor in the $CO_{(2)}RR$ to rationalize product distribution on various products.[9,21] Thus, adsorption site, strength, coverage and reactivity of CO_{ad} on the surface of Cu-based catalysts constitute a key set of variables in rationalizing reported reactivity and kinetic behaviors of the CO_2RR.[22] In addition, the CORR, aside from being an important reaction in its own right,[23−25] has been recognized as a convenient and informative model reaction for the CO_2RR, as the interfacial concentration of CO is unaffected by the multiple aqueous equilibria among dissolved CO_2, bicarbonate, carbonate and hydroxide in the electrolyte.[15] Recent studies provide evidence that the presence of CO_2 impacts the rate of the CORR, and this complexity will be discussed in detail in Section 4.3.

Many mechanistic interpretations of the Cu-catalyzed $CO_{(2)}RR$ are predicated on the presumed high coverage of CO_{ad} (θ_{CO}); however, experimental determination of θ_{CO} on

Received: August 22, 2023
Revised: October 5, 2023
Accepted: October 5, 2023
Published: October 26, 2023

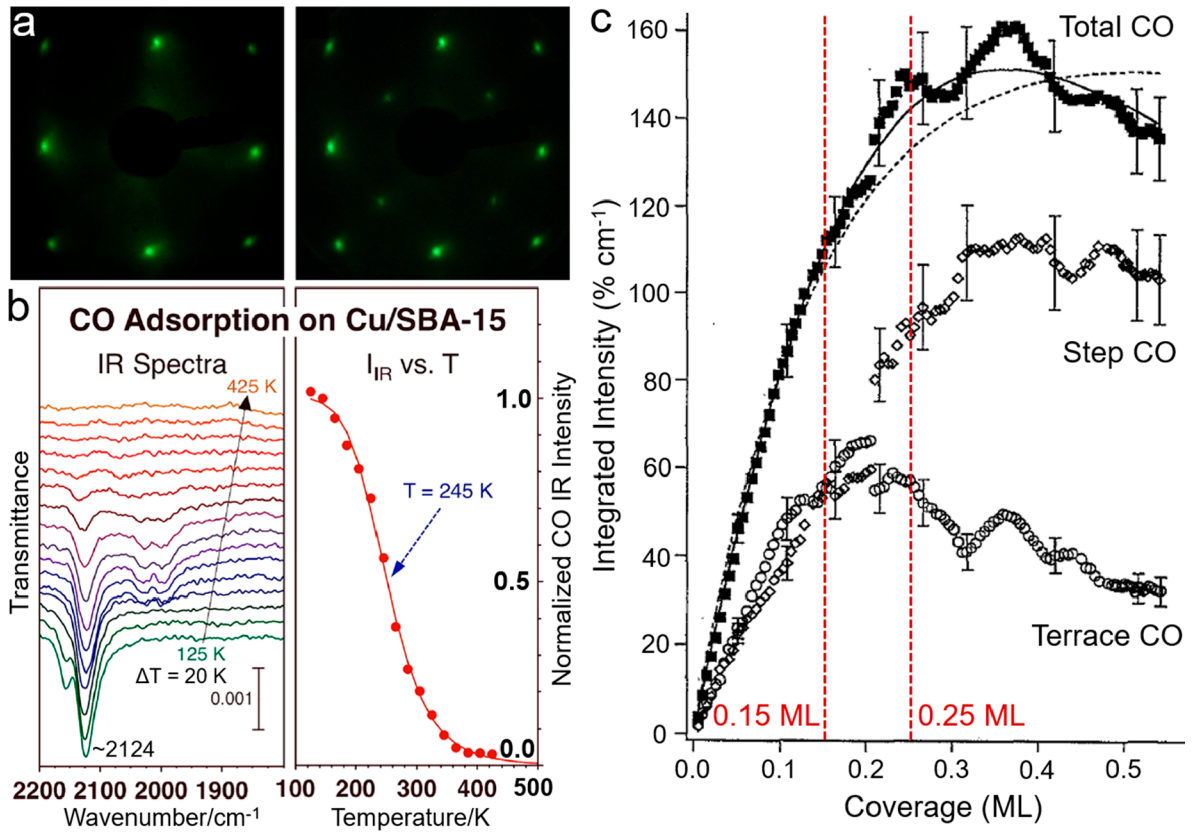

Figure 1. (a) Left: LEED patterns of the clean and ordered, as-prepared Cu(100) surface at room temperature. Right: the $c(2 \times 2)$CO overlayer at 120 K after ~40 L CO exposure. Reproduced with permission from ref 38. Copyright 2019 American Chemical Society. (b) Left: transmission IR spectra for CO adsorbed on a 5 wt % Cu/SBA-15 catalyst as a function of temperature during heating under vacuum, after initial adsorption at 125 K in 50 Torr of CO. Right: normalized peak intensity for the main feature in the IR spectra at 2124 cm^{-1} as a function of temperature, together with a fit to a sigmoidal curve. Reproduced with permission from ref 39. Copyright 2022 American Chemical Society. (c) Integrated IR peak intensity of CO as a function of coverage. Model fits to the total integrated intensity as a function of total coverage are also indicated. Reproduced with permission from ref 30. Copyright 1994 AIP Publishing.

Cu at electrochemical interfaces remains challenging and rare. The suppression of the hydrogen evolution reaction (HER) on Cu in the presence of concurrent $CO_{(2)}RR$ has been intuitively attributed to site blocking of CO_{ad}, which is considered as indirect evidence supporting high θ_{CO}, as well as an important reason for Cu to achieve high Faradaic efficiencies (FEs) for carbonaceous products in the $CO_{(2)}RR$.[26,27] For the site-blocking mechanism to fully account for the suppressed HER (by up to ~90%), close to complete coverage of CO_{ad} is expected,[26] while the saturated θ_{CO} on single crystal Cu facets was determined to be ~0.5 monolayer (ML).[28−30] In addition, multiple studies proposed that high θ_{CO} was key to facilitating carbon−carbon coupling in the formation of C_{2+} products.[19,31,32] For instance, Li et al. designed molecule-metal catalyst interfaces with a reaction-intermediate-rich local environment to improve the electrosynthesis of ethanol in the CO_2RR. High θ_{CO} was claimed to favor the carbon−carbon coupling and steer the reaction pathway toward ethanol over ethylene.[19] Computational modeling has become an indispensable technique to gain molecular level mechanistic information on the $CO_{(2)}RR$, in which a relatively high θ_{CO} is often implicitly assumed by placing two CO_{ad} on neighboring sites within relatively small repeating supercells to determine the energy barrier of the carbon−carbon coupling step.[21,33−35] Despite the prominence of θ_{CO} in the mechanistic deductions, its experimental determination on Cu surfaces under electrochemical conditions remains rare due to technical difficulties.

Recently, we reported experimental evidence suggesting that θ_{CO} on Cu surfaces is likely to be quite low at electrochemical conditions relevant to the $CO_{(2)}RR$ (~0.05 ML at 1.0 atm of CO).[18,36,37] These results highlight the need to revisit the mechanistic discussion predicated upon a high θ_{CO}, which is the main topic of this Perspective. This review first presents an overview of the experimental measurements of θ_{CO} on Cu surfaces, with a special focus on electrochemical systems, which is followed by discussion of mechanistic implications of low θ_{CO} in the context of reported reactivity and kinetic results of the $CO_{(2)}RR$. Finally, outlooks on future efforts for catalyst design and completing our mechanistic understanding of the $CO_{(2)}RR$ are discussed.

2. DETERMINING ABSOLUTE CO_{ad} COVERAGES ON COPPER SURFACES

In this section, we first briefly summarize earlier surface science studies of determining absolute CO_{ad} coverages on Cu surfaces under the ultrahigh vacuum (UHV) conditions or at solid−gas interfaces, then discuss recent efforts on estimating absolute CO_{ad} coverages on Cu electrodes at electrochemical conditions.

https://doi.org/10.1021/jacsau.3c00494
JACS Au 2023, 3, 2948−2963

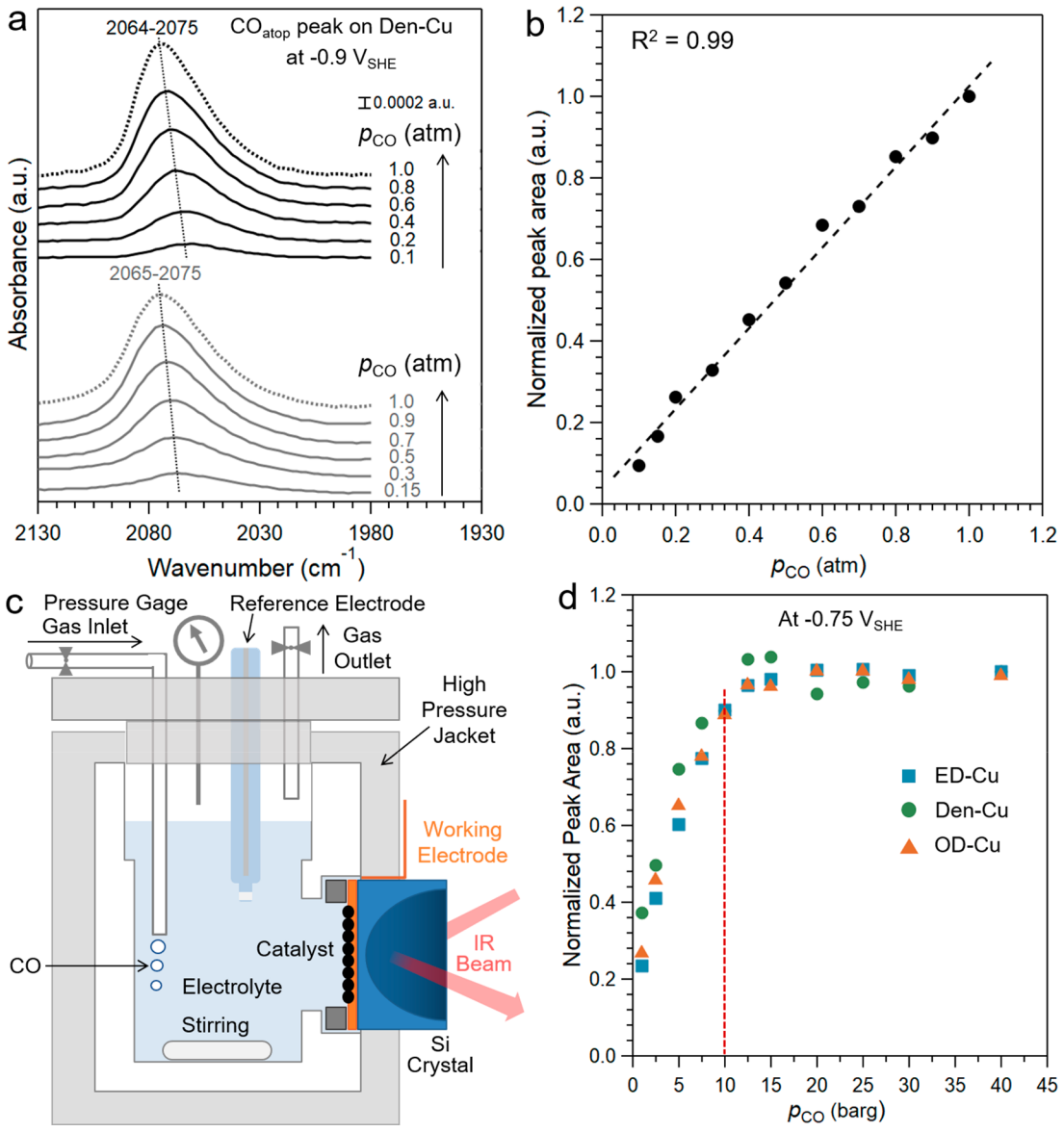

Figure 2. (a) In situ SEIRA spectra of CO adsorption on the Den-Cu electrode at −0.9 V_{SHE} in 1.0 M $NaHCO_3$ (pH 9.0) under different CO partial pressures indicated in the Figure. (b) CO adsorption isotherm on the Cu electrode at electrochemical conditions. Reproduced with permission from ref 18. Copyright 2022 John Wiley and Sons. (c) Schematic of the cathodic compartment of the custom-designed high-pressure spectroelectrochemical cell for SEIRAS. (b) Normalized CO peak area (to the peak area at 40 barg of CO) vs CO pressure. SEIRAS of CO adsorption on ED-Cu, Den-Cu, and OD-Cu was conducted at −0.75 V_{SHE} in 0.5 M $KHCO_3$ at different CO pressures. Reproduced with permission from ref 37. Copyright 2023 John Wiley and Sons.

2.1. CO Adsorption on Cu Surfaces at Solid/Gas Interfaces

Adsorption of CO on single crystalline Cu surfaces has been thoroughly investigated in the surface science literature with a number of quantitative experimental techniques, including low-energy electron diffraction (LEED), thermal desorption spectroscopy (TDS), infrared reflection absorption spectroscopy (IRAS), and surface potential measurements.[28,30,38,39] The short penetration depths of low energy electrons make LEED sensitive to the periodicity of the surface overlayer structure composed of adsorbates, from which the absolute coverage of adsorbates could be determined.[40] The pristine Cu(100) surface shows an expected square LEED pattern (Figure 1a left), and additional diffraction features appear after the introduction of an excess amount of CO, which is characteristic of a $c(2 \times 2)$ overlayer of adsorbates (Figure 1a right).[38,41] A saturated CO coverage of 0.5 monolayer (ML) could be inferred on Cu(100) (Figure 1a, right). In another study, a $R30°$ $(7\sqrt{2} \times \sqrt{2})$ LEED pattern of CO_{ad} was identified on Cu(100), leading to an estimated coverage of 0.57 ML.[42] Absolute CO coverages on Cu(111) and Cu(110) were determined with LEED to be 0.52 and 0.5 ML, respectively.[28,29] It should be noted that 1.0 ML of CO_{ad} is not achieved on any of the single crystal Cu facets, suggesting that it is quite difficult, if not impossible, to completely cover all surface Cu atoms with CO even with excess CO and in the absence of coadsorbates.

Relative CO coverages on Cu can also be determined by TDS and IR techniques.[30,39,43,44] Neither TDS nor IR can obtain the absolute θ_{CO} on its own. To determine absolute θ_{CO}, the signal intensity of mass spectrometry (MS) and IR for CO needs to be calibrated to those with a known θ_{CO}, i.e., a surface with a well-defined LEED pattern, to obtain the

https://doi.org/10.1021/jacsau.3c00494
JACS Au 2023, 3, 2948−2963

proportionality coefficient for MS and the extinction coefficient for IR spectroscopy. There are two common advantages of TDS and IR compared to LEED: (1) they could be applied to surfaces other than single crystal surfaces; and (2) they are able to gain information on the adsorption strength (enthalpy) on the adsorbates. Transmission IR spectra of CO adsorbed on 5 wt % Cu/SBA-15 show multiple bands in the 1900−2200 cm^{-1} region (Figure 1b left), corresponding to CO adsorbed on various types of Cu sites. For example, it is well-established that atop-bonded CO (CO_{atop}) on the terrace sites of Cu produces a C≡O stretching band ∼30 cm^{-1} lower in frequency compared with that of CO adsorbed on low-coordinated defect sites. The main peak at 2124 cm^{-1} observed in the temperature range of 125 to ∼350 K could be assigned to CO adsorption on low-coordinated metallic Cu atop site.[20,45−47] The higher wavenumber of the C≡O stretching mode on low-coordinated sites than that on terrace sites on Cu is unusual, which has been rationalized by combined effect of the dative bonding from the 5σ orbital of CO to the metal and the charge transfer from the metal to the adsorbed CO via the backbonding.[48] The relative CO coverage, as measured by the integrated area of the CO band (normalized to the peak centered at 2124 cm^{-1}), decreases with temperature, from which the CO adsorption enthalpy could be calculated with the Van't Hoff equation.[39] CO adsorption enthalpies on single crystal Cu surfaces were measured in the range of −46 to −84 kJ/mol, while those on the supported Cu particles exhibit a larger range of variation (−18 to −82 kJ/mol). The less negative CO adsorption enthalpies determined on supported Cu catalysts (∼ −20 kJ/mol) could be attributed, at least in part, to the presence of positively charged Cu species.[49]

The dynamical dipole coupling effect of adsorbed CO on Cu could complicate the quantification of relative CO coverages. Reliable quantification of θ_{CO} requires a known, and preferably linear, correlation between the spectral signal and θ_{CO}. Among the techniques capable of determining (relative) θ_{CO} discussed above, IR is the most widely employed for its accessibility and versatility. LEED can only be employed on single crystal surfaces under UHV, which limits its applications to practical catalysts. While TDS in principle works on both single crystal surfaces and high surface area catalysts, deconvolution of desorbed CO from the metal surface and the support could be tricky. In contrast, IR is able to not only determine the relative θ_{CO} based on the integrated area of the corresponding band, but also identify CO adsorbed on different types of surface sites. The linear correlation between the integrated peak area and surface coverage using IR spectroscopy with different configurations, e.g., transmission, reflection, and attenuated total reflection (ATR), is based on the Beer−Lambert law, which does not take lateral interactions among adsorbates into account. Coupling between neighboring CO_{ad} on Cu was reported to have a sizable impact on the IR intensity of the corresponding absorption band, which became increasingly significant at higher CO coverages, i.e., the dynamical dipole coupling effect.[28,30] Borguet and Dai investigated the spectroscopic behavior of CO adsorption on a stepped Cu(100) surface with different θ_{CO}, and found that integrated CO peak area started to deviate from linearity at θ_{CO} > 0.15 ML and exhibited a plateau at θ_{CO} > 0.25 ML (Figure 2c).[30] In addition, the IR bands corresponding to CO adsorbed on terrace and step sites exhibit different trends at θ_{CO} > 0.15 ML (Figure 1c), suggesting that quantification with IR at high CO coverage must be treated with caution.

2.2. CO Adsorption on Cu Surfaces at Electrochemical Conditions

Investigating CO adsorption at electrochemical conditions is considerably more complex than at the solid/gas or solid/vacuum interfaces.[50] Adsorption of CO dissolved in the electrolyte to the electrode surface is intrinsically a displacement reaction by nature, as the electrode surface is fully covered by interfacial water (assuming no specifically adsorbed ionic species) prior to CO adsorption. Thus, the energetics of CO adsorption at the electrochemical interface involve not only the interactions between CO and the surface but also the energetic cost of displacing a certain number of adsorbed water molecules as well as that of the associated structural change in the electric double layer (EDL). Generally, the adsorption of CO on Cu at the electrochemical interface is expected to be significantly weaker than under vacuum because of the favorable interaction between water and the Cu surface.[51−53] Recent studies determined the relative θ_{CO} on Cu at different electrode potentials using Raman spectroscopy.[54,55] Since the surface enhancement in Raman is highly dependent on the local roughness and structure,[56] significant variations in the intensity of the CO_{ad} band on the same catalyst sampled at different micrometer-sized spots with confocal Raman spectroscopy have been reported.[14] Thus, significant technical barriers need to be addressed before Raman spectroscopy could be considered as a reliable quantitative technique to determine θ_{CO}.[14,57]

We recently developed a strategy based on the surface-enhanced infrared absorption spectroscopy (SEIRAS) to determine the relative coverage of CO_{ad} on Cu surfaces with dendritic, spherical, and oxide-derived morphologies. The CO adsorption isotherm on a commercial dendritic Cu (Den-Cu) electrode was obtained at −0.9 V vs standard hydrogen electrode (V_{SHE}) by varying the CO partial pressures (p_{CO}) from 0.1 to 1.0 atm.[18] No appreciable CO consumption via its reduction reaction occurs at −0.9 V_{SHE} in 1.0 M $NaHCO_3$ (pH 9.0), so that the adsorption equilibrium could be reached by allowing sufficient time at each p_{CO}. Multiple reports claimed that only CO_{ad} in the atop configuration on Cu identified by SEIRAS is active in the CORR, while the bridge-bonded CO are spectators.[58,59] Thus, further analysis was performed only on the atop-bonded CO_{atop} band (Figure 2a). The integrated area of the CO_{atop} band exhibits a linear correlation with p_{CO}, indicative of a Henry type adsorption isotherm (Figure 2b). This is a strong indication that even at a p_{CO} of 1.0 atm, the absolute θ_{CO} remains low so that the site exclusion requirement in Langmuirian isotherms has not started to impact the adsorption. Comparison between the CO adsorption isotherms on Cu at UHV (Figure 1c) and electrochemical conditions (Figure 2b) suggests that the absolute CO coverage under the electrochemical conditions is below the θ_{CO} threshold beyond which the dynamical dipole coupling causes substantial deviations from the linear correlation between the peak area and θ_{CO}. Assuming this threshold is comparable under UHV and at electrochemical conditions, θ_{CO} at 1.0 atm of CO at −0.9 V_{SHE} on Cu could be roughly estimated to be at or below 0.15 ML (red dashed line in Figure 1c).[30,38,42] In addition to the adsorption isotherm, experiments in which CO_{ad} was switched from $^{12}CO_{ad}$ to $^{13}CO_{ad}$ also support the conclusion of low absolute θ_{CO} on Cu electrode at electrochemical conditions by the lack of the intensity borrowing effect.[18,30]

https://doi.org/10.1021/jacsau.3c00494
JACS Au 2023, 3, 2948−2963

To further narrow the range of θ_{CO} on Cu electrodes, higher CO pressures are needed to reach the θ_{CO} range within which the dynamical dipole coupling effect becomes appreciable. We designed and constructed a two-compartment stirred high-pressure spectroelectrochemical cell for SEIRAS capable of operating at CO pressures up to 60 barg (Figure 2c).[36,37] CO adsorption experiments were conducted on three different types of Cu surfaces, i.e., electrodeposited Cu (ED-Cu), commercial Den-Cu, and oxide-derived Cu (OD-Cu), at −0.75 V_{SHE} in 0.5 M $KHCO_3$ (pH 8.9). The integrated area of the CO_{atop} band on all three Cu surfaces investigated shows a similar trend within the p_{CO} range of 0.5 atm to 40 barg, with a linear rise at p_{CO} up to 10 barg before leveling off at higher p_{CO} (Figure 2d). The deviation from the linear correlation between p_{CO} and the peak area around 10 barg of CO is more likely caused by the dynamical dipole coupling effect than the saturation of CO_{ad} (~0.5 ML). Assuming a similar threshold θ_{CO} for significant dynamical dipole to that in Figure 1c, θ_{CO} at 10 barg of CO should be ~0.15 ML. It can be inferred that θ_{CO} at 1.0 atm of CO to be around 0.05 ML based on the linear isotherm at lower p_{CO}. Even with the unlikely assumption that the dynamical dipole coupling effect is absent at p_{CO} up to 40 barg and a saturation θ_{CO} (0.5 ML) is reached on Cu at p_{CO} above 10 barg, θ_{CO} at 1 atm of CO would still be ~0.15 ML. In another high-pressure study using a phosphate electrolyte, the saturation θ_{CO} on Den-Cu at 1.0 atm of CO was determined to be less than 0.05 ML at −0.6 V vs reversible hydrogen electrode (V_{RHE}), and further decreased to below 0.005 mL at −0.9 V_{RHE} due to the intense consumption of CO_{ad} via reduction reaction.[36] Thus, θ_{CO} on Cu surfaces at electrochemical interfaces at commonly employed p_{CO} (1.0 atm) appears to be quite low (~0.05 ML), which motivates us to revisit some reported $CO_{(2)}$RR mechanisms in Section 3. Further, similar CO adsorption isotherms can be found on three types of Cu surfaces with dendritic, spherical and oxide-derived morphologies, suggesting the generality of the low CO coverage on Cu surfaces, though the formation of C_{2+} products is preferred on OD-Cu compared to the other two Cu surfaces under identical conditions.[37] It is important to note that the direct comparison of peak intensity on different catalyst films in SEIRAS experiments is unreliable to calculate the relative surface coverage of adsorbates due to varying surface enhancement effects. The normalized peak area employed in Figure 2d indicates similar adsorption isotherms on ED-Cu, Den-Cu, and OD-Cu surfaces rather than comparable θ_{CO} on these three surfaces.

Measured CO adsorption enthalpy is consistent with the low θ_{CO} on Cu surfaces under electrochemical conditions. The standard CO adsorption enthalpy (ΔH°_{CO}) on Cu surfaces at electrochemical interface could be determined with SEIRAS by varying temperature (Figure 3a and b) in an approach similar to that discussed in the previous section (Figure 1b).[37] The excellent linearity between p_{CO} and the peak area, denoted as $A(T)$ at temperature T, at p_{CO} below 1.0 atm (Figure 2a) makes the quantification of relative θ_{CO} reliable. ΔH°_{CO} could be deduced from relation between logarithm of the integrated area of the CO_{ad} peak at a specific temperature ($\ln[A(T)]$) vs $1/T$ (Figure 3c). ΔH°_{CO} of CO adsorption on Den-Cu is determined to be 1.5 ± 0.5 kJ mol^{-1}.[37] This value is significantly more positive than that observed under UHV conditions, where the ΔH°_{CO} of CO on the supported Cu particles was estimated to be in the range of −18 to −82 kJ/mol.[39,49,60] The slightly positive ΔH°_{CO} value of CO on Cu at the electrochemical interface is an indication that the adsorption of CO on Cu at the electrochemical interface is much less favorable than that under vacuum, which is consistent with the low θ_{CO} on Cu surfaces at electrochemical conditions. The significantly weakened CO adsorption under electrochemical conditions could be attributed to the competive adsorption of other surface species, such as water or oxygen-containing species ($CuO_x(OH)_y$), as reported in recent studies.[13,14,61,62] Even in the absence of specific water adsorption on the Cu surface, as suggested in a recent computational study,[63] the insertion of CO_{ad} between the first layer of water and the electrode surface would necessarily incur an energy cost, thereby weakening the CO adsorption. In addition, the CO desorption kinetics has also been employed in determining the relative CO binding strengths on different surfaces.[64]

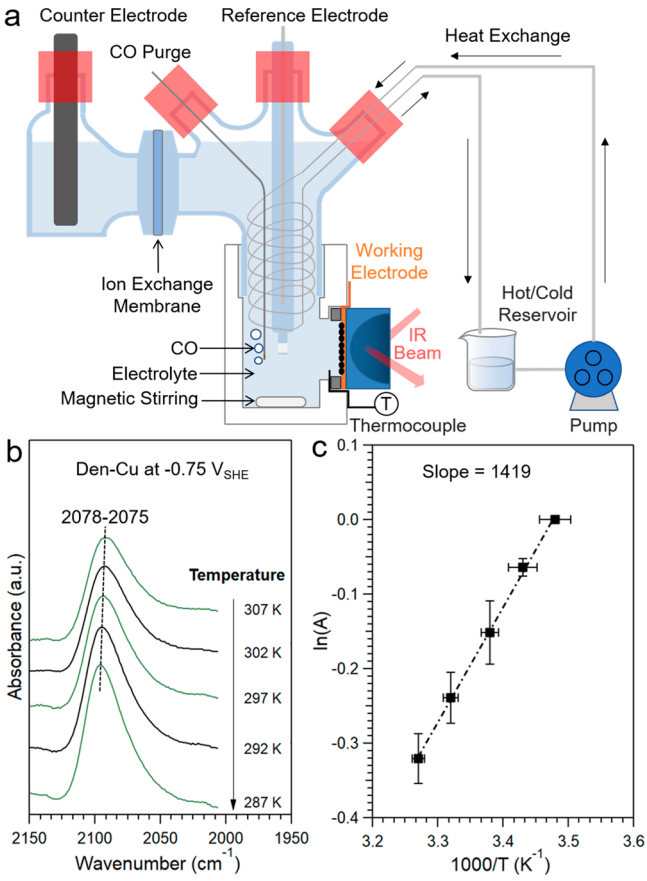

Figure 3. (a) Schematic of the homemade two-compartment, three-electrode SEIRAS capable of varying the electrolyte temperature. (b) In situ SEIRA spectra of CO adsorption on Den-Cu at −0.75 V_{SHE} in 0.5 M $KHCO_3$ at different temperatures. (c) Semilog plot of normalized integrated CO peak area in (b) vs 1000/T. Error bars were calculated based on variations in three independent measurements. Reproduced with permission from ref 37. Copyright 2023 John Wiley and Sons.

3. MECHANISTIC IMPLICATIONS OF LOW CO COVERAGES

In light of the low θ_{CO} on Cu surfaces at conditions relevant to the $CO_{(2)}$RR discussed in the previous section, there is a need to revisit reported mechanisms that implicitly or explicitly assume a relatively high θ_{CO}.

https://doi.org/10.1021/jacsau.3c00494
JACS Au 2023, 3, 2948−2963

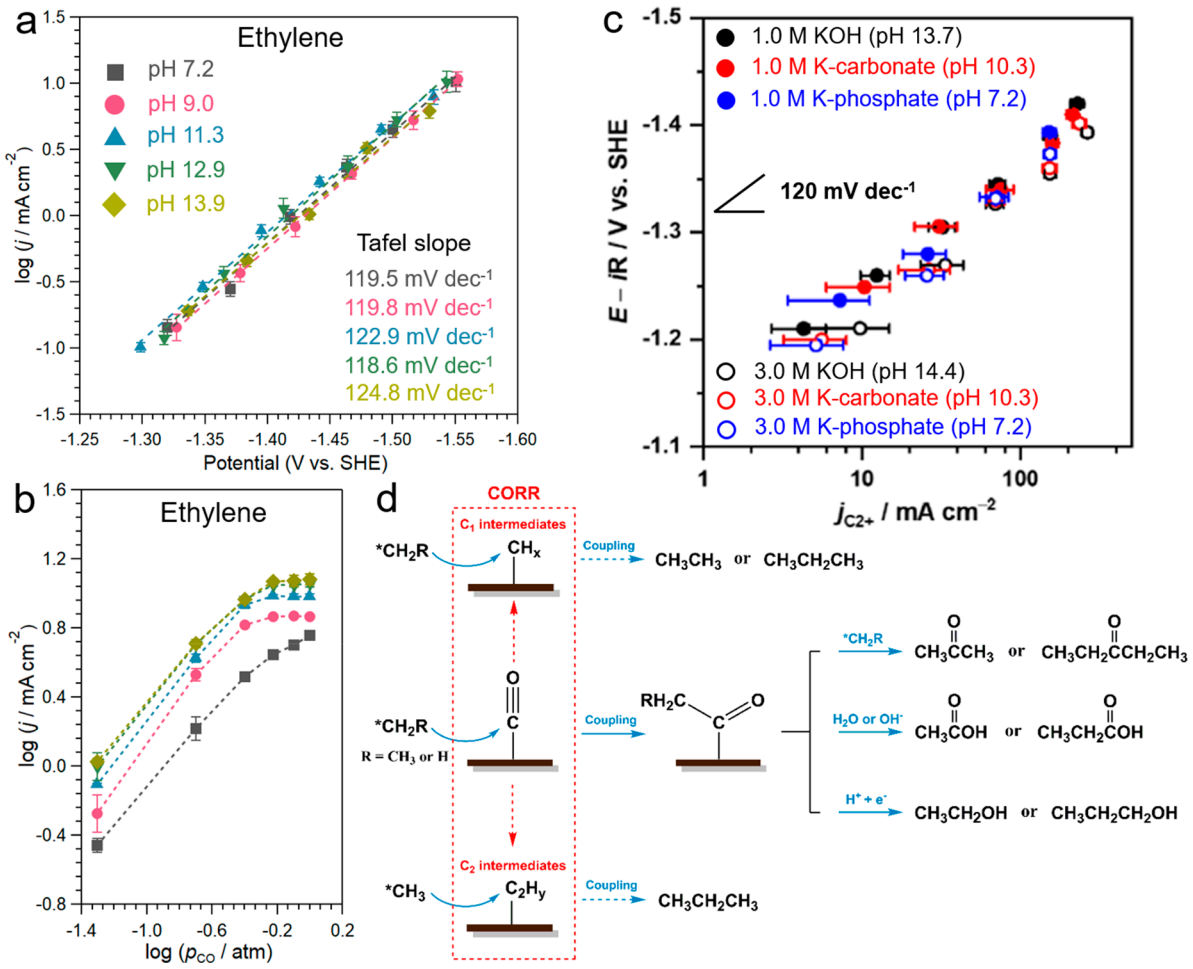

Figure 4. (a) Tafel curves for ethylene at different electrolyte pH values with a p_{CO} of 0.3 atm in an H-cell. The logarithms of partial current densities for ethylene are plotted on the SHE scale. (b) p_{CO} dependence for ethylene in different electrolyte pH values at −1.5 V_{SHE}. The logarithms of partial current densities for ethylene versus logarithms of p_{CO}. Reproduced with permission from ref 18. Copyright 2022 John Wiley and Sons. (c) Tafel curves for the total C_{2+} products in various electrolytes at ambient temperature and p_{CO} by a gas-fed flow cell. Reproduced with permission from ref 68. Copyright 2023 American Chemical Society. (d) Schematic of the proposed reaction pathway through the addition of alkyl species into the CORR system. Reproduced with permission from ref 73. Copyright 2022 American Chemical Society.

3.1. Rate-Determining Step in the Formation of Multicarbon Products

The rate and selectivity control in the formation of C_{2+} products in the $CO_{(2)}RR$ have been the focus of a significant fraction of recent reports in the field due to their high economic values.[3] Since it takes many elementary steps to convert CO_{ad} into C_{2+} products, it is key to identify the rate-determining step (RDS) in the reaction network to guide the catalyst design. A multitude of possible elementary steps have been computed with density functional theory (DFT) based methods. Coupling of two adsorbed CO_{ad} stands out as the favored RDS candidate on Cu surfaces with the lowest calculated activation barrier.[21,65−67] Reaction pathways with hydrogenation of CO_{ad} occurring prior to the formation of the C−C bond typically involve a higher calculated barrier than the CO_{ad} dimerization.[21,67] The hypothesis of CO_{ad} dimerization as the RDS in the formation of C_{2+} products leads to a number of experimentally verifiable electrokinetic predictions: 1) formation rate of C_{2+} products is independent of the electrolyte pH, because neither H^+ nor OH^- participates in the RDS or prior steps; 2) the Tafel slope for all C_{2+} products is ∼120 mV/dec because CO_{ad} dimerization is the first electron transfer step in the reaction network; and 3) a second order reaction for CO_{ad} because the dimerization involves two CO_{ad} species. The first two predictions have been verified by electrokinetic studies.[18,24,68] The formation rates of C_{2+} products on Den-Cu employed in Figures 2 and 3 were comparable in the pH range 7−14 when the reactions were conducted at the same absolute potentials, i.e., referenced to the standard hydrogen electrode (SHE), with the effect of the internal resistance properly corrected (Figure 4a). We note that the local pH at the electrochemical interface during the $CO_{(2)}RR$ is expected to be elevated compared to that of the bulk electrolyte due to the generation of OH^- in the cathodic reaction. This effect is expected to be less severe in more alkaline electrolytes due to the high absolute OH^- concentration. The fact that pH-dependence was observed over the entire pH range of 7−14 suggests the deviation of the interfacial pH from the bulk value is not a significant factor in these electrokinetic studies. In addition, it has been demonstrated that the deviation of interfacial pH from the bulk electrolyte becomes insignificant with sufficient buffering capacity.[24] Tafel slopes of ∼120 mV/dec were determined for all of the C_{2+} products. The remarkable agreement between the results obtained in the H-type (Figure 4a)[24] and flow-type reactors (Figure 4c)[68] suggests that reliable kinetic data could

https://doi.org/10.1021/jacsau.3c00494
JACS Au 2023, 3, 2948−2963

Table 1. CO Reaction Orders for C_{2+} Product Formation Determined in Different Reactor Configurations on Cu-Based Electrocatalysts

Reactor configuration	CO reaction order for C_{2+} products	Conditions	ref
H-cell	1st at $p_{CO} \leq 0.4$ atm 0th at 0.6 atm < p_{CO} < 1.0 atm	At −1.5 V_{SHE} and ambient temperature in 1.0 M Na^+ electrolytes with varying pH values ranging from 7.2 to 13.9	18
	~0th at 0.1 atm < p_{CO} < 1.0 atm	At −1.96 V vs Ag/AgCl and −35 °C in 0.1 M LiTFSI/EtOH	65
Flow cell	1st at 0.02 atm < p_{CO} < 0.4 atm 0th at 0.4 atm < p_{CO} < 1.0 atm	At −1.41 V_{SHE} and ambient temperature in 1.0 M KOH catholyte	68
	1st at p_{CO} < 0.25 atm 0th at 0.25 atm < p_{CO} < 1.0 atm	At −1.0 V_{RHE} and ambient temperature in 1.0 M KOH catholyte	69
	1st at 0 atm < p_{CO} < 0.15 atm ~0th at 0.3 atm < p_{CO} < 1.0 atm	At −0.6 V_{RHE} and ambient temperature in 1.0 M KOH catholyte	70
MEA	1st at 0.02 atm < p_{CO} < 0.2 atm 0th at 0.2 atm < p_{CO} < 5.0 atm	At 2.2 V cell potential and ambient temperature using 0.1 KOH as anolyte	68

be collected in either type of cells as long as the mass transport limitation of CO to the electrocatalyst is effectively alleviated.

Measured reaction orders of CO in the CORR on Cu are inconsistent with the hypothesis that the coupling of two CO_{ad} species is the RDS. Reaction orders of CO in the CORR has been determined in the H-type,[24,65] the flow-type and the membrane electrode assembly (MEA) configurations,[68−70] with highly consistent results (Table 1). Formation rates of C_{2+} products increase linearly at low p_{CO} (≤0.4 atm), indicating a first order reaction. The CO reaction order gradually drops to close to zero as p_{CO} approaches 1.0 atm (Figure 4b). It should be noted that the hypothesis of CO_{ad} coupling as the RDS predicts a second order for CO_{ad}, rather than the gas phase CO. Thus, the correlation between p_{CO} and θ_{CO} on Cu at electrochemical conditions is needed to determine the reaction order of CO_{ad} from that of gas phase CO. The Henry type adsorption isotherm of CO on Cu at the electrochemical interface (Figure 2b), together with the lack of the dynamical dipole coupling at the low θ_{CO}, indicates a linear correlation between p_{CO} and θ_{CO}. It follows that the reaction orders of CO_{ad} and gas phase CO should be identical, i.e., between 0 and 1. This result directly contradicts the prediction based on the hypothesis of the CO_{ad}-CO_{ad} coupling being the RDS. In fact, the RDS involving the coupling of any two C_1 species would lead to a second order reaction for CO with a low θ_{CO}. Assuming all elementary steps prior to the RDS involving C−C coupling are pseudo-equilibrated, all C_1 species are in equilibrium with gas phase CO:

$$CO_g \leftrightarrow CO_{aq} \leftrightarrow CO_{ad} \leftrightarrow (H)_x CO_{ad} \leftrightarrow CH_{x,ad} \quad (1)$$

Spectroscopic results suggest that CO_{ad} is the most abundant adsorbed intermediates in the $CO_{(2)}$RR on Cu surfaces.[71,72] A low θ_{CO} entails coverages of other adsorbed C_1 species are even lower, thus excluding site competition among different adsorbed C_1 species. It follows that coverages of adsorbed C_1 species are proportional to one another via equilibria. In addition, the coverage of any adsorbed C_1 species is proportional to the activity of the dissolved CO_{aq} via the adsorption/desorption equilibrium between CO_{aq} and CO_{ad}. Consequently, either a Langmuir−Hinshelwood type coupling between two surface-bound C_1 species or an Eley−Rideal type coupling between one adsorbed C_1 species and a CO_{aq} molecule would lead to a second order reaction with respect to CO. Therefore, an important mechanistic consequence for the low θ_{CO} on Cu surface, in light of the measured CO reaction orders, is that C−C coupling is unlikely to be the RDS in the formation of C_{2+} products.[18] Further, our recent study determined that the reaction order of CO is below unity at p_{CO} up to 60 barg.[36] Even these measured CO reaction orders likely overestimate the true values due to the mass transport limitation of CO. The Cu catalysts employed in the high-pressure study do not have the gas diffusion configuration, which tends to slow the transport of CO to the Cu surface. The infrared CO_{ad} band almost disappears at −0.9 V_{RHE} at atmospheric pressure of CO, indicating that the transport of CO to the Cu surface cannot keep up with its consumption in the CORR on this electrode. Thus, the CO reaction order in the CORR on Cu is consistently below unity in the p_{CO} range between 0.4 atm and 60 barg. The close-to-unity CO reaction order at p_{CO} lower than 0.4 atm indicates that CO hydrogenation is likely the RDS, while the origin of the subunity order at p_{CO} above 0.6 atm is less clear (Figure 4b). One possible explanation is that only adsorbed water is able to function as the proton source in the CO hydrogenation. A higher θ_{CO} leads to a lower coverage of adsorbed water capable of donating protons, which could lower the reaction order of CO.[18]

The discrepancy between the RDS predicted by electrokinetic and computational investigations could be rationalized by the low θ_{CO} on Cu surfaces at $p_{CO} \leq 1.0$ atm. The lower calculated energy barrier of the coupling between two neighboring CO_{ad} species is energetically more facile than the hydrogenation of CO_{ad}. Low θ_{CO} on Cu leads to low probability of two CO_{ad} species encountering on the surface, while CO_{ad} is surrounded by water, the proton source in its hydrogenation. Rates measured in electrokinetic experiments reflect the characteristics of the most populated pathway in the reaction network. It is likely that CO hydrogenation is the more populated pathway even though its activation barrier is slightly higher than the C−C coupling. Our recent study reported a case in which the coverages of intermediates played the decisive role in determining the product distribution.[73] Adsorbed alkyl groups could be introduced to the Cu surface by the corresponding alkyl iodides and are able to couple with CO_{ad}. Coupling of $C_nH_{2n+1,ad}$ with CO_{ad} forms the surface bound alkylcarbonyl before further coupling with either water or another CO_{ad} to yield the corresponding organic acid or ketone (Figure 4d). Importantly, the coupling of the adsorbed

https://doi.org/10.1021/jacsau.3c00494
JACS Au 2023, 3, 2948−2963

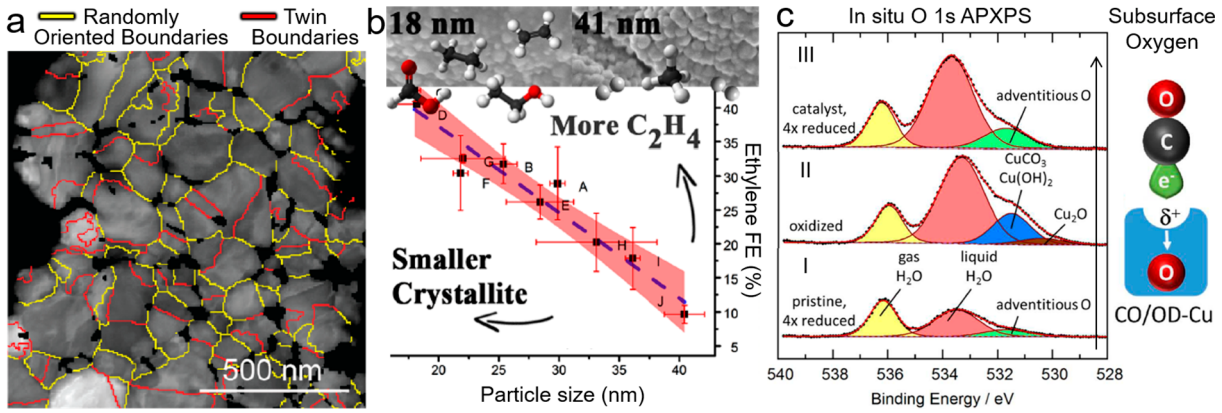

Figure 5. (a) Transmission electron microscopy (TEM) image quality maps with overlaid boundaries of OD-Cu. Reproduced with permission from ref 74. Copyright 2012 American Chemical Society. (b) FE of ethylene in the CO_2RR on OD-Cu as a function of particle size. Reproduced with permission from ref 76. Copyright 2016 American Chemical Society. (c) In situ O 1s ambient pressure X-ray photoelectron spectroscopy (APXPS) spectra of pristine Cu foil (I), oxidized Cu foil (II), and OD-Cu (III). The presence of subsurface oxygen (right) is supported by adventitious O in OD-Cu (green area in APXPS). Reproduced with permission from ref 77. Copyright 2017 American Chemical Society.

alkyl group and CO_{ad} could occur at potentials too positive for the CORR, i.e., 0 to −0.3 V_{RHE}, suggesting that the coupling pathway involves only a modest activation barrier. $CH_{3,ad}$ was captured in the CORR on Cu at −0.7 V_{RHE} when CO is co-electrolyzed with CD_3I, suggesting that $CH_{3,ad}$ and CO_{ad} coexist on the Cu surface at the reaction conditions. However, no detectable level of the coupling product acetone was formed despite the modest barrier, which is attributed to the low $CH_{3,ad}$ coverage during the CORR. Thus, the formation rate of coupling products could be limited by either the surface coverage of the reactants or the associated reaction barrier. The measured reaction orders of CO in the Cu-catalyzed CORR suggest that the low θ_{CO} makes hydrogenation of CO_{ad} the favored pathway.

3.2. θ_{CO}-Activity Correlations

Much recent research effort has been devoted to enhancing the activity and selectivity for high value product in the $CO_{(2)}RR$ on Cu-based catalysts through a variety of synthetic and postsynthetic treatment strategies, and variations in the CO binding strength and θ_{CO} are often cited as the cause to the observed changes in performance.[3,5] Simple oxidation−reduction treatment of polycrystalline Cu yields the oxide-derived Cu, often referred to as OD-Cu, which shows significantly lower overpotentials required to generate C_{2+} products in the $CO_{(2)}RR$.[23,74] Although the composition and structure of sites generated in the redox treatment responsible for the enhanced activity remain a topic of discussion in the literature, major schools of thoughts correlate the $CO_{(2)}RR$ performance on OD-Cu with sites with higher affinity to CO. Kanan and colleagues attributed the high CORR activity on OD-Cu to surface sites originating from disordered surfaces at grain boundaries, which had a stronger binding to CO_{ad} and enhanced the steady-state CO_{ad} coverage (Figure 5a).[23,75] Temperature-programmed desorption experiments showed that CO desorbed at higher temperature on OD-Cu than the polycrystal Cu surface.[75] Yeo and co-workers reported that the selectivity toward ethylene in the CO_2RR exhibited a clear correlation with the crystallite size of Cu particles (Figure 5b), where smaller particles had higher availability and more diverse sites for CO adsorption leading to a higher θ_{CO} for ethylene formation.[76] Nilsson and co-workers reported a significant amount of residual subsurface oxygen in OD-Cu (Figure 5c), which generated active sites with elevated CO binding energy and θ_{CO}, thus promoting the formation of C_{2+} products.[77] In light of the close-to-zero reaction order of CO_{ad} discussed in the previous section at the commonly employed p_{CO} in the CORR (1.0 atm), an increased θ_{CO} alone is unlikely the main cause for any major enhancement in the CORR activity on Cu. Meanwhile, θ_{CO} is closely related to the CO binding strength of the sites, which has been proposed to be a descriptor for the intrinsic activity in the CORR. It should be noted that most CO energies reported in the literature were based on DFT calculations, where many of the complexities associated with electrochemical interfaces, e.g., water and ions, were not taken into consideration. With the advent of the SEIRAS-based method (Figure 3), ΔH°_{CO} became an experimentally accessible variable. The measured ΔH°_{CO} on OD-Cu (−2.0 kJ/mol) is slightly more negative than that of polycrystal Cu (1.5 kJ/mol), suggesting a possible role of ΔH°_{CO} in determining the intrinsic activity of Cu sites.[37] However, a correlation between ΔH°_{CO} and the $CO_{(2)}RR$ based on data from the two catalysts is far from reliable. Additional results from Cu-based catalysts with different compositions and structures are needed to verify this correlation. Moreover, smaller crystallites were reported to possess higher rates and FE for ethylene production when normalized to the geometric area of the catalyst layer.[76] Since smaller particles generally have larger surface areas, and thus another possible cause for the higher activity in OD-Cu could be the higher specific surface area than the polycrystal Cu due to the redox treatment. However, the observed lower onset potential for the CORR on OD-Cu than polycrystalline Cu cannot be explained by the difference in surface areas.[57]

Aside from OD-Cu, higher θ_{CO} is also regarded as a likely casue for enhanced performance on other Cu-based in the $CO_{(2)}RR$. Sargent and co-workers demonstrated that the modification of Cu electrodes with organic molecules could effectively regulate the distribution of $CO_{(2)}RR$ products toward C_{2+} species.[19,78] The enhanced performance is rationalized by the ability of molecular adsorbates to generate a high density of CO_{ad} and facilitate C−C coupling. Similar findings were recently reported by Zhao et al., and the latest advances in the participation of surface decorating molecules in $CO_{(2)}RR$ to C_{2+} products have been summarized by Chen et al.[79,80] Moreover, Cu-based bimetallic materials, such as the Cu−Pd electrocatalyst developed by Ma et al.[81] and Ji et al.,[82]

https://doi.org/10.1021/jacsau.3c00494
JACS Au 2023, 3, 2948−2963

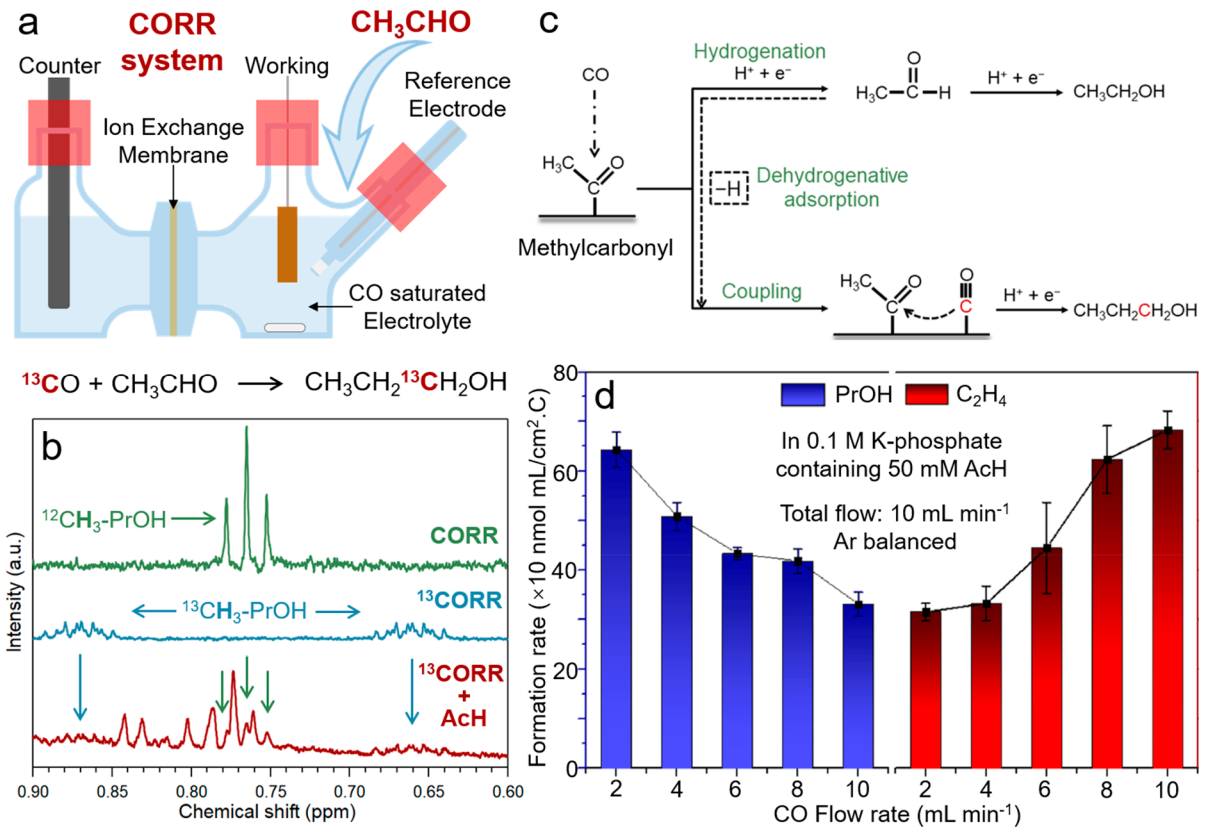

Figure 6. (a) Schematic of the co-electrolysis of CO with AcH in an H-cell. (b) ^{1}H NMR features corresponding to the terminal $-CH_3$ groups in PrOH produced from the CORR (green), the ^{13}CORR (blue), and the ^{13}CORR with 10 mM AcH (red). The reactions were conducted in 0.1 M KOH at -0.6 V_{RHE}. (c) Schematic of the proposed reaction network and the cross-coupling between ^{13}CO and AcH. Reproduced with permission from ref 17. Copyright 2020 American Chemical Society. (d) Formation rates of PrOH (blue) and ethylene (red) at different CO flow rates balanced with Ar to a total flow rate of 10 mL min^{-1}. Electrolyte: 50 mM AcH in 0.1 M K-phosphate buffer. Reproduced with permission from ref 88. Copyright 2023 American Chemical Society.

were shown to facilitate the production of C_{2+} products, which were rationalized by the enhanced CO_{ad} adsorption and increased θ_{CO}. Xie et al. identified the Mg−Cu bimetallic catalyst as an effective catalyst in the CO_2RR to C_{2+} products, exhibiting an FE of 80% and a current density of 1.0 A cm^{-2} at -0.77 V_{RHE} in the flow cell configuration. In situ spectroelectrochemical analyses revealed that Mg^{2+} species could stabilize Cu^{+} sites during the CO_2RR, and the promoted C−C coupling was attributed to the increase in θ_{CO}.[83] Given the close-to-zero reaction order of CO_{ad} at a p_{CO} of 1.0 atm regardless of the reactor configurations (Table 1), increased θ_{CO} alone is unlikely to be the main reason for the significantly enhanced formation of C_{2+} products on Cu-based catalysts. Other contributing factors need to be identified in future investigations.

4. CO-ELECTROLYSIS AS A STRATEGY FOR MECHANISTIC STUDIES

Section 3 discusses two key features of Cu-catalyzed $CO_{(2)}$RR: (1) the RDS occurs as the first electron and proton transfer step in the conversion of CO_{ad}; and (2) coverage of all carbon-containing adsorbates, including CO_{ad}, is relatively low. These two features made mechanistic investigations of the $CO_{(2)}$RR challenging, as they render two of the most potent experimental approaches largely ineffective beyond the very beginning of the reaction network. Electrokinetic results cannot provide information on the reaction network beyond the RDS, and low coverage makes it challenging to identify any adsorbed intermediates other than CO_{ad} with in situ spectroscopic methods. So far, proposed reaction networks are largely based on deductions from the product distributions determined at different potentials and computational modeling, which are revealing but lack of direct experimental verification. In this section, we discuss the co-electrolysis strategy reported in the recent literature capable of gaining mechanistic insights into the Cu-catalyzed $CO_{(2)}$RR beyond the early RDS.

4.1. Co-Electrolysis of CO and Precursors to Reaction Intermediates

One effective strategy to probe the reaction network after the RDS is to co-electrolyze CO with a suspected reaction intermediate. The rationale with this approach is that if the added chemical is indeed a reaction intermediate, the yield for the product formed by the coupling between CO and this intermediate would be significantly higher than in the CORR. Koper and co-workers conducted the reduction of small C_1 and C_2 organic molecules, such as formaldehyde, glyoxal, glycolaldehyde, etc., to identify potential intermediates in $CO_{(2)}$RR.[84] The formation and consumption of intermediates were monitored by online MS as a function of potential. CHO_{ad} was identified as the key intermediate toward methane formation, and the initial step for ethylene generation was CO_{ad} dimerization followed by the formation of enediol, enediolate or oxametallacycle. It was also found that both

https://doi.org/10.1021/jacsau.3c00494
JACS Au 2023, 3, 2948−2963

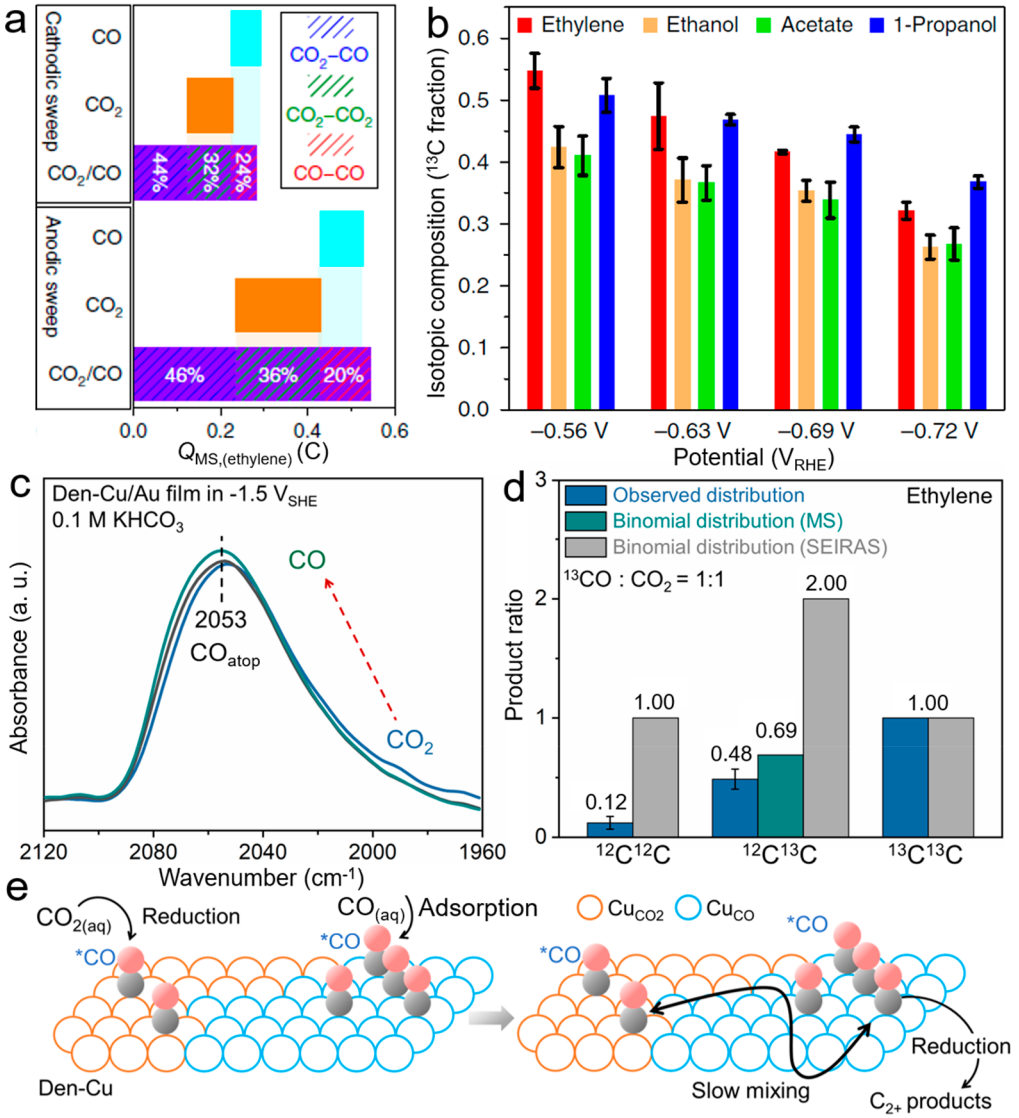

Figure 7. (a) DEMS-derived ethylene mass charges for the three different feeds during the cathodic and anodic voltammetric sweep. The purple ethylene charge bars are divided into the relative contributions of each ethylene formation pathway (blue, green, and red hashed patterns) confirmed by DEMS. The orange and cyan bars are the ethylene charge by the pure CO_2 and CO feeds, respectively. Reproduced with permission from ref 90. Copyright 2019 Springer Nature. (b) Isotopic composition of ethylene, ethanol, acetate, and PrOH produced by the co-electrolysis of $^{13}CO/^{12}CO_2$ (7:3) mixture on OD-Cu at different potentials. Reproduced with permission from ref 91. Copyright 2019 Springer Nature. (c) In situ SEIRA spectra of CO_{ad} with the atmosphere gradually switching from CO_2 (blue) to CO (green). (d) Observed distribution (blue bars) and expected binomial distributions of isotopologues of ethylene produced based on the $^{12}CH_2{}^{12}CH_2/^{13}CH_2{}^{13}CH_2$ ratio determined by MS (green bars), and $^{12}CO_{ad}/^{13}CO_{ad}$ ratio determined by SEIRAS (gray bars) in the co-electrolysis of $^{13}CO/^{12}CO_2$ (0.5 atm/0.5 atm) on Den-Cu at −1.5 V_{SHE} in 0.1 M $KHCO_3$. (e) Schematic of the proposed two-site model on Cu. Reproduced with permission from ref 93. Copyright 2023 Springer Nature.

glyoxal and glycolaldehyde were first reduced to acetaldehyde (AcH) at −0.35 V_{RHE}, and then further converted to ethanol at −0.6 V_{RHE}, suggesting that AcH served as the precursor to ethanol and was a potential intermediate in the $CO_{(2)}$RR on Cu. Furthermore, Clark and Bell confirmed this hypothesis via differential electrochemical mass spectrometry (DEMS) with high surface sensitivity. They reported evidence that AcH was a crucial intermediate product in the CO_2RR and acted as the precursor to ethanol and n-propanol (PrOH).[85]

We conducted co-electrolysis of CO and AcH to understand the pathway leading to PrOH, the most commonly observed C_3 product in the $CO_{(2)}$RR (Figure 6a).[17] Isotopic labeling experiments of ^{13}CO co-electrolysis with CH_3CHO exhibited the coexistence of ^{12}C and ^{13}C in the $-CH_3$ group of the produced PrOH, as indicated by the observation of both triplet (green arrows, corresponding to $-{}^{12}CH_3-$PrOH) and multiplet (blue arrows, corresponding to $-{}^{13}CH_3-$PrOH) in ^1H NMR spectrum (red curve, Figure 6b). This is a strong indication that a portion of PrOH is produced via the cross-coupling between CO and AcH, since AcH is the exclusive source of ^{12}C in the co-electrolysis and no PrOH is generated in the reduction of AcH.[84,86] The triplet in the ^1H NMR spectrum corresponding to $-{}^{12}CH_2OH$ is absent and only $-{}^{13}CH_2OH$ exists in the produced PrOH from ^{13}CO-AcH co-electrolysis. These findings indicate that the carbon atom in the $-{}^{13}CH_2OH$ group in PrOH, including those produced via the C−C coupling between CO and AcH, derives exclusively from CO (chemical equation in Figure 6b). Moreover, the

https://doi.org/10.1021/jacsau.3c00494
JACS Au 2023, 3, 2948−2963

carbon atom in AcH attacked by CO during their C−C coupling process is identified to be the carbonyl carbon (−CHO) via the co-electrolysis of perdeuterated AcH and CO.[17] It should be noted that any stable chemical that can be co-electrolyzed with CO is more likely to be a precursor to a reaction intermediate than a reaction intermediate. This is because for surface mediated electrocatalytic reactions such as the $CO_{(2)}RR$, reaction intermediates are likely reactive adsorbed species rather than stable (commercially available) chemicals. Once an adsorbed species is desorbed, the probability that it readsorbs on the surface and couples with other surface bound species is much lower. In addition, many adsorbed species cannot desorb without chemical transformations, e.g., $CH_{3,ad}$. Therefore, surface adsorbed methylcarbonyl ($-COCH_3$) formed through the dehydrogenative adsorption of AcH or CORR in the co-electrolysis was proposed to be the key intermediate for ethanol and PrOH generation (Figure 6c),[17] which is reminiscent of the coupling reactions on Au surfaces.[87] Recently, Koper and co-workers further demonstrated the competitive adsorption between CO_{ad} and adsorbed methylcarbonyl in the co-electrolysis of CO and AcH, which could impact the formation of PrOH during the $CO_{(2)}RR$ on Cu.[88] Interestingly, the highest PrOH formation rate was observed at the lowest CO flow rate (2 mL min^{-1}) in a 50 mM AcH phosphate buffer electrolyte (blue bars, Figure 6d). While an increase in AcH concentration up to 600 mM in a CO-saturated phosphate buffer electrolyte resulted in a greater formation of PrOH. These observations suggest that CO could impede the adsorption and conversion of AcH, and achieving an optimal balance between CO and AcH near the electrode surface is needed to promote the PrOH formation. The increase in p_{CO} in 50 mM AcH-containing electrolyte enhances ethylene production (red bars, Figure 6d), indicating that methylcarbonyl is not the precursor for its formation. In addition, in a 0.1 M KOH electrolyte without AcH, ethanol production is minimal at intermediate p_{CO}, while PrOH production reaches its maximum. This observation indicates that methylcarbonyl is an intermediate for the formation of both molecules, thereby supporting the proposed mechanism in Figure 6c. The impact of CO and AcH concentrations on the PrOH formation in the co-electrolysis highlights the challenge of achieving a high FE for PrOH in the $CO_{(2)}RR$: HER will dominate the reaction at low p_{CO}, while the preferential adsorption of CO_{ad} over methylcarbonyl at high p_{CO} will compromise their coupling to generate PrOH.[88]

4.2. Capturing Elusive Adsorbed Intermediates via Co-electrolysis

A key flaw in the approach of co-electrolysis of CO with (the precursor to) a suspected reaction intermediate is that the reaction intermediate may or may not be formed in the $CO_{(2)}RR$. For example, there is no guarantee that methylcarbonyl is formed in the CORR on Cu in the absence of externally introduced AcH, and the formation of PrOH could proceed from an entirely different pathway, e.g., coupling of three CO_{ad} before hydrodeoxygenation and hydrogenation steps (though unlikely based on electrokinetic results discussed in the previous section). Thus, capturing surface bound reactive intermediates is key to understanding the reaction network, which is challenging due to their low surface coverages. An example of this is to introduce chemically distinct probe species such as alkyl groups via the ready dissociation of alkyl iodides on the Cu surface.[89] Co-electrolysis of CO and alkyl iodides was reported to capture adsorbed C_1 and C_2 intermediates in Cu-catalyzed CORR by the derived alkyl groups.[73] Surface-bound alkyl groups ($C_nH_{2n+1,ad}$) formed in the co-electrolysis are able to couple with CO_{ad} to produce carboxylates and ketones via one and two successive nucleophilic attacks (Figure 4d), respectively. Importantly, surface adsorbed CH_x ($x \leq 3$) and C_2H_x ($x \leq 4$) intermediates generated during the CORR are also successfully intercepted and identified to be the precursors for methane and PrOH formation, respectively. The introduction of the probing species, e.g., alkyl iodides, ideally only perturbs the reaction of interest slightly without changing the reaction network under investigation in any substantial way, e.g., product distribution and formation rates, to ensure that the intercepted intermediates belong to the reaction network of interest rather than caused by the perturbation.

4.3. Co-electrolysis of CO and CO_2

The CO_2RR to valuable chemicals is widely believed to proceed via two consecutive and orthogonal steps, i.e., the CO_2-to-CO conversion and the CORR.[3,5] However, the orthogonality of the two reaction steps has been challenged by Strasser and co-workers.[90] They observed an increased ethylene production when CO and CO_2 were cofed on a Cu-based catalyst, compared to the individual feeding of either CO or CO_2. Time-resolved isotope-labeling experiments of $^{12}CO_2/^{13}CO$ (1:3) co-electrolysis conducted via an operando DEMS during cyclic voltammetric sweep demonstrated that the enhanced ethylene production primarily originated from a CO_2−CO cross-coupling reaction pathway, accounting for ∼45% of the total (blue hashed patterns, Figure 7a). Taking those produced via CO self-coupling into consideration, approximately two-thirds (∼67%) of the total ethylene yield involved CO from the external source (rather than produced from CO_2 reudction) in the co-electrolysis (blue + red hashed patterns, Figure 7a). Moreover, the presence of CO in the feed was able to sustain a high rate of CO_2 conversion even at the most cathodic electrode potentials where local reactant depletion occurs under the pure CO_2 feed. The authors hypothesized, based on largely computational results, that CO_2-to-CO and CO-to-C_{2+} conversions occurred on distinct Cu sites, with these two types of sites being atomically mixed to facilitate rapid diffusion of CO_{ad} produced from the CO_2RR toward sites responsible for its coupling with CO_{ad} from gas feed.

Lum and Ager pioneered the analysis of isotopologue distributions of C_2 products in the co-electrolysis of $^{13}CO/^{12}CO_2$ mixtures on Cu.[91] Regardless of the reaction mechanisms and the identity of the RDS, C_2 products must form through the coupling of two C_1 species. Thus, the distribution of isotopologues reveals the source of carbon atoms in the C_2 products. A binomial distribution is expected if all surface sites are equivalent or if C_1 species diffuse efficiently on the surface so that the $^{12}C_1$ and $^{13}C_1$ species distribution on each type of site is consistent with the overall statistical distribution. Thus, the comparison of the observed and the binomial distributions of isotopologues, as well as the isotopic distributions in the products, could provide otherwise inaccessibile mechanistic insights regarding the site heterogeneity on Cu surfaces. Lum and Ager found that the isotopic compositions (^{13}C fraction) of ethanol and acetate are identical regardless of the potential (Figure 7b) in the $^{13}CO/^{12}CO_2$ (7:3) co-electrolysis on OD-Cu, which strongly

https://doi.org/10.1021/jacsau.3c00494
JACS Au 2023, 3, 2948−2963

suggests that these two products are generated from the same active sites. While ethylene is produced from a different set of active sites, as evidenced by its consistently higher ^{13}C fraction. The ^{13}C fraction of PrOH appears distinct from either that of ethylene or of ethanol/acetate (Figure 7b), indicating that PrOH is generated on another set of active sites.[91] Similar observations were made by Ling et al. in the co-electrolysis of a different isotopic labeling gas mixture of $^{12}CO/^{13}CO_2$ on a CuAg catalyst.[92] Interestingly, there is no preferential inclusion of ^{12}C or ^{13}C in either the methyl or carboxylate (hydroxymethylene) carbon in acetate (ethanol), suggesting against the possibility that the methyl group is formed in a specific type of site before coupling with CO.

Recently, through a combination of in situ SEIRAS and co-electrolysis studies of $^{13}CO/^{12}CO_2$ mixtures, we show that CO_2 has a promotional effect on the CORR on Cu, and there are at least two distinct types of Cu sites.[93] An ∼90% increase in the production rate of overall C_{2+} products was observed when increasing the CO_2 fraction in the feed from 0 to 20% while keeping the CO fraction at 80% with balancing Ar. Complementary SEIRAS conducted under identical conditions exhibited a negligible increase in the CO_{ad} peak area upon switching the atmosphere from CO_2 to CO (Figure 7c), suggesting that variations in θ_{CO} were unlikely to be the primary cause of the enhanced C_{2+} production rates. Interestingly, co-electrolysis of $^{13}CO/^{12}CO_2$ (1:1) mixtures confirmed that the majority of ethylene was derived from the C−C coupling of two C_1 species derived from ^{13}CO, as indicated by the high fraction of $^{13}CH_2{}^{13}CH_2$ among the isotopologues of ethylene (blue bars in Figure 7d), which differs from previous observations by Strasser and co-workers.[90] SEIRA spectrum collected under the same condition exhibited comparable peak areas for $^{12}CO_{ad}$ and $^{13}CO_{ad}$, suggesting that $^{13}CO_{ad}$ was more active in the CORR. Based on the significant deviation of the observed distribution of ethylene isotopologues from the binomial distribution (Figure 7d), we propose a two-site model, in which one type of site is active for CORR (Cu_{CO}), while the other favors the CO_2-to-CO conversion but remains relatively inert toward further CO conversion (Cu_{CO2}), to account for the site heterogeneity on Cu (Figure 7e). Quantitative analysis of the spectroscopic and co-electrolysis results indicates that CO adsorbed on Cu_{CO} is at least six times more active in the CORR than that on Cu_{CO2} sites.[93] Co-electrolysis experiments conducted on Cu(111) and Cu(100) facets indicate that Cu_{CO2} and Cu_{CO} sites correspond to Cu(111)-like and undercoordinated Cu sites, respectively. The discrepancy in the CO_2−CO coupling ratios observed in ethylene between Strasser's and our work could be attributed to the different relative densities of the Cu_{CO} and Cu_{CO2} sites. In addition, Wei et al. observed a selectivity shift from ethylene to acetate as the major product with an increase of p_{CO} in 1.0 atm CO/CO_2 cofeed, and this trend is further enhanced at higher CO pressure (0.4 MPa).[94] A positive correlation between the product distribution and the CO adsorption configuration identified by operando Raman spectroscopy was obtained. Ethylene selectivity was found to correlate with the percentage of CO_{ad} on bridge and hollow sites (referred to as CO_{bridge} and CO_{hollow}, respectively), while acetate production exhibited a strong correlation with CO_{atop} percentage, also suggesting the crucial role of surface sites in the $CO_{(2)}RR$.

5. SUMMARY AND OUTLOOK

Surface coverage of CO_{ad} plays a pivotal role in determining both reaction activity and product distribution of the electrochemical $CO_{(2)}RR$. Although CO adsorption properties on Cu have been extensively studied in UHV systems, experimental determinations of θ_{CO} and CO adsorption enthalpy on Cu-based electrodes under electrochemical conditions remain rare. A number of experimental techniques based on SEIRAS were recently developed, which suggest θ_{CO} to be ∼0.05 ML under electrochemical conditions at 1.0 atm. Additionally, the CO adsorption enthalpy on Den-Cu was estimated to be ∼1.5 kJ/mol. The high ΔH°_{CO} and low θ_{CO} on Cu electrodes necessitate a revisit of existing $CO_{(2)}RR$ mechanisms in the literature, including the RDS for C_{2+} product formation and the correlations between θ_{CO} and activity. Even with the low θ_{CO} and early RDS in the $CO_{(2)}RR$, co-electrolysis of CO and CO_2, CO and suspected reaction intermediates, as well as CO and nucleophilic reagents, is able to gain mechanistic insights into the Cu-catalyzed $CO_{(2)}RR$ beyond the early RDS. Despite recent advances in experimental techniques and mechanistic understanding, we are still far from a comprehensive and predictive mechanistic framework for the Cu-catalyzed $CO_{(2)}RR$. A few gaps in understanding and potential fruitful research directions are discussed below.

(1) Site heterogeneity. Recent mechanistic investigations highlight the site heterogeneity on Cu surfaces,[14,91,93] which is also expected on other Cu-based catalysts. The presence of sites with slightly different chemical properties on polycrystalline and OD-Cu surfaces should come as no surprise, because single crystal facets contain different sites, e.g., terrace, step, vacancy sites. However, the discovery of different groups of sites possessing distinct activities toward specific steps in the reaction network, e.g., the CO_2-to-CO conversion and further hydrogenation of CO, raises the question whether single descriptor such as the CO binding energy would be sufficient as a catalyst design principle. Different steps in the $CO_{(2)}RR$ network could have different optimal ΔH°_{CO} values. In addition, the mechanism through which popular strategies of introducing dopants and surface decorating agents enhance the $CO_{(2)}RR$ performance becomes more uncertain. Do these strategies introduce new types of active sites, modify the properties of existing sites, or merely change the distribution of different types of sites? Investigating the correlation between ΔH°_{CO} and the $CO_{(2)}RR$ performance on Cu-based catalysts with diverse compositions and structures, including single crystal facets of Cu, would provide insights into potential synergistic effects. In essence, site heterogeneity introduces an additional dimension in catalyst design. Further, understanding the effect of the surface reconstruction on ΔH°_{CO} and the catalytic performance of spent catalysts could be helpful in elucidating the catalyst deactivation mechanism. The only experimental method capable of determining ΔH°_{CO} at electrochemical conditions yields values that are weighted average of all present surface sites. Development of techniques with better resolving power, in terms of both energy and spatial resolution, for different types of sites would be highly desirable. In addition, understanding whether ΔH°_{CO} and distribution of

https://doi.org/10.1021/jacsau.3c00494
JACS Au 2023, 3, 2948−2963

different types of surface sites are independent variables could potentially reduce the dimension of the parameter space for catalyst optimization.

(2) Interdependene among different steps in the $CO_{(2)}RR$ network. The beneficial effect of CO_2 on the CORR weakens the argument of using the CORR as a model reaction to search and optimize CO_2RR catalysts. Meanwhile, elucidating the mechanism for the promotional effect of CO_2 could help catalyst and process design. For example, if CO_2 enhances the CORR by stabilizing intermediates or the activated complex, species either on the catalyst surface or in the electrolyte could be introduced to take full advantage of this promotional effect. In addition, the development of high spatial resolution characterization could contribute to the validation of the two-site model of Cu illustrated in Figure 7e, and further elucidate the interdependence between CO_2-to-CO conversion and CO reduction.

(3) Suppression of the HER at low CO coverage. An interesting observation is that the presence of CO_{ad} the $CO_{(2)}RR$ on Cu could substantially suppress the competing HER.[26,27] With the low θ_{CO} on Cu (~0.05 ML at 1.0 atm of CO), it remains unclear how such low θ_{CO} could suppress the HER that occurs on all Cu sites. Understanding the mechanism through which sparsely populated CO_{ad} affect the competing HER could shed light on the modes of interactions among species in the electric double layer. CO_{ad} could affect the activity of neighboring sites by either altering the charge distribution on the surface or via interactions with other interfacial species, e.g., cations. Thus, investigating the impacts of CO_{ad} on the HER in electrolytes containing varying cations would provide valuable insights.

AUTHOR INFORMATION

Corresponding Author

Bingjun Xu − *College of Chemistry and Molecular Engineering, Peking University, Beijing 100871, China;* orcid.org/0000-0002-2303-257X; Email: b_xu@pku.edu.cn

Authors

Xiaoxia Chang − *College of Chemistry and Molecular Engineering, Peking University, Beijing 100871, China*

Haocheng Xiong − *Department of Chemical Engineering, Tsinghua University, Beijing 100084, China*

Qi Lu − *Department of Chemical Engineering, Tsinghua University, Beijing 100084, China;* orcid.org/0000-0002-0380-2629

Complete contact information is available at: https://pubs.acs.org/10.1021/jacsau.3c00494

Notes

The authors declare no competing financial interest.

ACKNOWLEDGMENTS

This work is supported by Beijing National Laboratory for Molecular Sciences and the National Natural Science Foundation of China (grant number 21872079, 22278002, 8200906905 and 8206100474).

REFERENCES

(1) Chang, X.; Wang, T.; Gong, J. CO_2 photo-reduction: insights into CO_2 activation and reaction on surfaces of photocatalysts. *Energy Environ. Sci.* **2016**, *9* (7), 2177−2196.

(2) De Luna, P.; Hahn, C.; Higgins, D.; Jaffer, S. A.; Jaramillo, T. F.; Sargent, E. H. What would it take for renewably powered electrosynthesis to displace petrochemical processes? *Science* **2019**, *364* (6438), No. eaav3506.

(3) Nitopi, S.; Bertheussen, E.; Scott, S. B.; Liu, X.; Engstfeld, A. K.; Horch, S.; Seger, B.; Stephens, I. E. L.; Chan, K.; Hahn, C.; et al. Progress and Perspectives of Electrochemical CO_2 Reduction on Copper in Aqueous Electrolyte. *Chem. Rev.* **2019**, *119* (12), 7610−7672.

(4) Song, Y.; Xie, W.; Shao, M. Recent Advances in Integrated Electrode for Electrocatalytic Carbon Dioxide Reduction. *Acta Phys. -Chim. Sin.* **2021**, *38* (6), No. 2101028.

(5) Shi, Y.; Hou, M.; Li, J.; Li, L.; Zhang, Z. Cu-Based Tandem Catalysts for Electrochemical CO_2 Reduction. *Acta Phys. -Chim. Sin.* **2022**, *38* (11), No. 2206020.

(6) Hori, Y.; Kikuchi, K.; Suzuki, S. Production of CO and CH_4 in Electrochemical Reduction of CO_2 at Metal Electrodes in Aqueous Hydrogencarbonate Solution. *Chem. Lett.* **1985**, *14* (11), 1695−1698.

(7) Hori, Y.; Murata, A.; Takahashi, R.; Suzuki, S. Enhanced formation of ethylene and alcohols at ambient temperature and pressure in electrochemical reduction of carbon dioxide at a copper electrode. *J. Chem. Soc., Chem. Commun.* **1988**, 17−19.

(8) Wang, L.; Nitopi, S. A.; Bertheussen, E.; Orazov, M.; Morales-Guio, C. G.; Liu, X.; Higgins, D. C.; Chan, K.; Nørskov, J. K.; Hahn, C.; et al. Electrochemical Carbon Monoxide Reduction on Polycrystalline Copper: Effects of Potential, Pressure, and pH on Selectivity toward Multicarbon and Oxygenated Products. *ACS Catal.* **2018**, *8* (8), 7445−7454.

(9) Bagger, A.; Ju, W.; Varela, A. S.; Strasser, P.; Rossmeisl, J. Electrochemical CO_2 Reduction: A Classification Problem. *ChemPhysChem* **2017**, *18* (22), 3266−3273.

(10) Hori, Y. Electrochemical CO_2 Reduction on Metal Electrodes. *Modern aspects of electrochemistry*; Springer: New York, 2008; pp 89−189.

(11) Li, M.; Garg, S.; Chang, X.; Ge, L.; Li, L.; Konarova, M.; Rufford, T. E.; Rudolph, V.; Wang, G. Toward Excellence of Transition Metal-Based Catalysts for CO_2 Electrochemical Reduction: An Overview of Strategies and Rationales. *Small Methods* **2020**, *4* (7), No. 2000033.

(12) Bodappa, N.; Su, M.; Zhao, Y.; Le, J. B.; Yang, W. M.; Radjenovic, P.; Dong, J. C.; Cheng, J.; Tian, Z. Q.; Li, J. F. Early Stages of Electrochemical Oxidation of Cu(111) and Polycrystalline Cu Surfaces Revealed by in Situ Raman Spectroscopy. *J. Am. Chem. Soc.* **2019**, *141* (31), 12192−12196.

(13) Zhao, Y.; Chang, X.; Malkani, A. S.; Yang, X.; Thompson, L.; Jiao, F.; Xu, B. Speciation of Cu Surfaces During the Electrochemical CO Reduction Reaction. *J. Am. Chem. Soc.* **2020**, *142* (21), 9735−9743.

(14) Chang, X.; Zhao, Y.; Xu, B. pH Dependence of Cu Surface Speciation in the Electrochemical CO Reduction Reaction. *ACS Catal.* **2020**, *10* (23), 13737−13747.

(15) Dunwell, M.; Lu, Q.; Heyes, J. M.; Rosen, J.; Chen, J. G.; Yan, Y.; Jiao, F.; Xu, B. The Central Role of Bicarbonate in the Electrochemical Reduction of Carbon Dioxide on Gold. *J. Am. Chem. Soc.* **2017**, *139* (10), 3774−3783.

(16) Firet, N. J.; Smith, W. A. Probing the Reaction Mechanism of CO_2 Electroreduction over Ag Films via Operando Infrared Spectroscopy. *ACS Catal.* **2017**, *7* (1), 606−612.

(17) Chang, X.; Malkani, A.; Yang, X.; Xu, B. Mechanistic Insights into Electroreductive C−C Coupling between CO and Acetaldehyde into Multicarbon Products. *J. Am. Chem. Soc.* **2020**, *142* (6), 2975−2983.

(18) Chang, X.; Li, J.; Xiong, H.; Zhang, H.; Xu, Y.; Xiao, H.; Lu, Q.; Xu, B. C-C Coupling Is Unlikely to Be the Rate-Determining Step in the Formation of C_{2+} Products in the Copper-Catalyzed Electro-

https://doi.org/10.1021/jacsau.3c00494
JACS Au 2023, 3, 2948−2963

chemical Reduction of CO. *Angew. Chem., Int. Ed.* **2022**, *61* (2), No. e202111167.
(19) Li, F.; Li, Y. C.; Wang, Z.; Li, J.; Nam, D.-H.; Lum, Y.; Luo, M.; Wang, X.; Ozden, A.; Hung, S.-F.; et al. Cooperative CO_2-to-ethanol conversion via enriched intermediates at molecule−metal catalyst interfaces. *Nat. Catal.* **2020**, *3* (1), 75−82.
(20) Gunathunge, C. M.; Li, X.; Li, J.; Hicks, R. P.; Ovalle, V. J.; Waegele, M. M. Spectroscopic Observation of Reversible Surface Reconstruction of Copper Electrodes under CO_2 Reduction. *J. Phys. Chem. C* **2017**, *121* (22), 12337−12344.
(21) Montoya, J. H.; Shi, C.; Chan, K.; Norskov, J. K. Theoretical Insights into a CO Dimerization Mechanism in CO_2 Electroreduction. *J. Phys. Chem. Lett.* **2015**, *6* (11), 2032−2037.
(22) Xu, Y.; Yang, H.; Chang, X.; Xu, B. Introduction to Electrocatalytic Kinetics. *Acta Phys. -Chim. Sin.* **2022**, *39* (4), No. 2210025.
(23) Li, C. W.; Ciston, J.; Kanan, M. W. Electroreduction of carbon monoxide to liquid fuel on oxide-derived nanocrystalline copper. *Nature* **2014**, *508* (7497), 504−507.
(24) Li, J.; Chang, X.; Zhang, H.; Malkani, A. S.; Cheng, M.-J.; Xu, B.; Lu, Q. Electrokinetic and in situ spectroscopic investigations of CO electrochemical reduction on copper. *Nat. Commun.* **2021**, *12* (1), 3264.
(25) Liu, X.; Schlexer, P.; Xiao, J.; Ji, Y.; Wang, L.; Sandberg, R. B.; Tang, M.; Brown, K. S.; Peng, H.; Ringe, S.; et al. pH effects on the electrochemical reduction of $CO_{(2)}$ towards C_2 products on stepped copper. *Nat. Commun.* **2019**, *10* (1), 32.
(26) Hori, Y.; Murata, A.; Yoshinami, Y. Adsorption of CO, intermediately formed in electrochemical reduction of CO_2, at a copper electrode. *J. Chem. Soc., Faraday Trans.* **1991**, *87* (1), 125−128.
(27) Ooka, H.; Figueiredo, M. C.; Koper, M. T. M. Competition between Hydrogen Evolution and Carbon Dioxide Reduction on Copper Electrodes in Mildly Acidic Media. *Langmuir* **2017**, *33* (37), 9307−9313.
(28) Hollins, P.; Pritchard, J. Interactions of CO molecules adsorbed on Cu(111). *Surf. Sci.* **1979**, *89*, 486−495.
(29) Harendt, C.; Goschnick, J.; Hirschwald, W. The interaction of CO with copper (110) studied by TDS and LEED. *Surf. Sci.* **1985**, *152−153*, 453−462.
(30) Borguet, E.; Dai, H.-L. Site-specific properties and dynamical dipole coupling of CO molecules adsorbed on a vicinal Cu(100) surface. *J. Chem. Phys.* **1994**, *101* (10), 9080−9095.
(31) Huang, Y.; Handoko, A. D.; Hirunsit, P.; Yeo, B. S. Electrochemical Reduction of CO_2 Using Copper Single-Crystal Surfaces: Effects of CO* Coverage on the Selective Formation of Ethylene. *ACS Catal.* **2017**, *7* (3), 1749−1756.
(32) Tan, Y. C.; Lee, K. B.; Song, H.; Oh, J. Modulating Local CO_2 Concentration as a General Strategy for Enhancing C−C Coupling in CO_2 Electroreduction. *Joule* **2020**, *4* (5), 1104−1120.
(33) Dinh, C. T.; Burdyny, T.; Kibria, M. G.; Seifitokaldani, A.; Gabardo, C. M.; Garcia de Arquer, F. P.; Kiani, A.; Edwards, J. P.; De Luna, P.; Bushuyev, O. S.; et al. CO_2 electroreduction to ethylene via hydroxide-mediated copper catalysis at an abrupt interface. *Science* **2018**, *360* (6390), 783−787.
(34) Cheng, T.; Xiao, H.; Goddard, W. A. Nature of the Active Sites for CO Reduction on Copper Nanoparticles; Suggestions for Optimizing Performance. *J. Am. Chem. Soc.* **2017**, *139* (34), 11642−11645.
(35) Ma, W.; Xie, S.; Liu, T.; Fan, Q.; Ye, J.; Sun, F.; Jiang, Z.; Zhang, Q.; Cheng, J.; Wang, Y. Electrocatalytic reduction of CO_2 to ethylene and ethanol through hydrogen-assisted C−C coupling over fluorine-modified copper. *Nat. Catal.* **2020**, *3* (6), 478−487.
(36) Hou, J.; Chang, X.; Li, J.; Xu, B.; Lu, Q. Correlating CO Coverage and CO Electroreduction on Cu via High-Pressure in Situ Spectroscopic and Reactivity Investigations. *J. Am. Chem. Soc.* **2022**, *144* (48), 22202−22211.
(37) Xiong, H.; Sun, Q.; Chen, K.; Xu, Y.; Chang, X.; Lu, Q.; Xu, B. Correlating the Experimentally Determined CO Adsorption Enthalpy with the Electrochemical CO Reduction Performance on Cu Surfaces. *Angew. Chem., Int. Ed.* **2023**, *62* (10), No. e202218447.
(38) Roiaz, M.; Falivene, L.; Rameshan, C.; Cavallo, L.; Kozlov, S. M.; Rupprechter, G. Roughening of Copper (100) at Elevated CO Pressure: Cu Adatom and Cluster Formation Enable CO Dissociation. *J. Phys. Chem. C* **2019**, *123* (13), 8112−8121.
(39) Han, T.; Lee, I.; Cao, Y.; Zhou, X.; Zaera, F. Thermodynamics of Carbon Monoxide Adsorption on Cu/SBA-15 Catalysts: Under Vacuum versus under Atmospheric Pressures. *J. Phys. Chem. C* **2022**, *126* (6), 3078−3086.
(40) Zanazzi, E.; Bardi, U.; Maglietta, M. On the reliability of intensity measurements for surface structure analysis by LEED. *J. Phys. C: Solid State Phys.* **1980**, *13* (20), 4001−4006.
(41) Persson, B. N. J.; Ryberg, R. Vibrational interaction between molecules adsorbed on a metal surface: The dipole-dipole interaction. *Phys. Rev. B* **1981**, *24* (12), 6954−6970.
(42) Tracy, J. C. Structural Influences on Adsorption Energy. III. CO on Cu(100). *J. Chem. Phys.* **1972**, *56* (6), 2748−2754.
(43) Collins, D. M.; Spicer, W. E. The adsorption of CO, O_2, and H_2 on Pt. *Surf. Sci.* **1977**, *69* (1), 85−113.
(44) Yu, K. Thermal desorption studies of CO and H_2 from the Cu-Ni alloy. *J. Catal.* **1976**, *44* (3), 373−384.
(45) Pritchard, J.; Catterick, T.; Gupta, R. K. Infrared spectroscopy of chemisorbed carbon monoxide on copper. *Surf. Sci.* **1975**, *53* (1), 1−20.
(46) Nielsen, N. D.; Smitshuysen, T. E. L.; Damsgaard, C. D.; Jensen, A. D.; Christensen, J. M. Characterization of oxide-supported Cu by infrared measurements on adsorbed CO. *Surf. Sci.* **2021**, *703*, 121725.
(47) Hadjiivanov, K.; Knözinger, H. FTIR study of CO and NO adsorption and coadsorption on a Cu/SiO_2 catalyst: Probing the oxidation state of copper. *Phys. Chem. Chem. Phys.* **2001**, *3* (6), 1132−1137.
(48) Hollins, P. The influence of surface defects on the infrared spectra of adsorbed species. *Surf. Sci. Rep.* **1992**, *16* (2), 51−94.
(49) Vollmer, S.; Witte, G.; Wöll, C. Determination of site specific adsorption energies of CO on copper. *Catal. Lett.* **2001**, *77* (1/3), 97−101.
(50) Chang, S.; Weaver, M. In Situ Infrared Spectroscopy at Single-Crystal Metal Electrodes: An Emerging Link between Electrochemical and Ultrahlgh-Vacuum Surface Science. *J. Phys. Chem.* **1991**, *95*, 5391−5400.
(51) Gunathunge, C. M.; Li, J.; Li, X.; Waegele, M. M. Surface-Adsorbed CO as an Infrared Probe of Electrocatalytic Interfaces. *ACS Catal.* **2020**, *10* (20), 11700−11711.
(52) Tang, Q.-L.; Chen, Z.-X. Density functional slab model studies of water adsorption on flat and stepped Cu surfaces. *Surf. Sci.* **2007**, *601* (4), 954−964.
(53) Castillo, J. M.; Vlugt, T. J. H.; Calero, S. Understanding Water Adsorption in Cu−BTC Metal−Organic Frameworks. *J. Phys. Chem. C* **2008**, *112* (41), 15934−15939.
(54) Jiang, S.; Klingan, K.; Pasquini, C.; Dau, H. New aspects of operando Raman spectroscopy applied to electrochemical CO_2 reduction on Cu foams. *J. Chem. Phys.* **2019**, *150* (4), No. 041718.
(55) Zhan, C.; Dattila, F.; Rettenmaier, C.; Bergmann, A.; Kuhl, S.; Garcia-Muelas, R.; Lopez, N.; Cuenya, B. R. Revealing the CO Coverage-Driven C-C Coupling Mechanism for Electrochemical CO_2 Reduction on Cu_2O Nanocubes via Operando Raman Spectroscopy. *ACS Catal.* **2021**, *11* (13), 7694−7701.
(56) Stiles, P. L.; Dieringer, J. A.; Shah, N. C.; Van Duyne, R. P. Surface-enhanced Raman spectroscopy. *Annu. Rev. Anal. Chem.* **2008**, *1*, 601−626.
(57) Chang, X.; He, M.; Lu, Q.; Xu, B. Origin and effect of surface oxygen-containing species on electrochemical CO or CO_2 reduction reactions. *Sci. China Chem.* **2023**, *66* (1), 96−106.
(58) Gunathunge, C. M.; Ovalle, V. J.; Li, Y.; Janik, M. J.; Waegele, M. M. Existence of an Electrochemically Inert CO Population on Cu Electrodes in Alkaline pH. *ACS Catal.* **2018**, *8* (8), 7507−7516.

https://doi.org/10.1021/jacsau.3c00494
JACS Au 2023, 3, 2948−2963

(59) Chang, X.; Vijay, S.; Zhao, Y.; Oliveira, N. J.; Chan, K.; Xu, B. Understanding the complementarities of surface-enhanced infrared and Raman spectroscopies in CO adsorption and electrochemical reduction. *Nat. Commun.* **2022**, *13* (1), 2656.
(60) Dandekar, A.; Vannice, M. A. Determination of the Dispersion and Surface Oxidation States of Supported Cu Catalysts. *J. Catal.* **1998**, *178* (2), 621−639.
(61) Sang, J.; Wei, P.; Liu, T.; Lv, H.; Ni, X.; Gao, D.; Zhang, J.; Li, H.; Zang, Y.; Yang, F.; et al. A Reconstructed $Cu_2P_2O_7$ Catalyst for Selective CO_2 Electroreduction to Multicarbon Products. *Angew. Chem., Int. Ed.* **2022**, *61* (5), No. e202114238.
(62) Duan, G. Y.; Li, X. Q.; Ding, G. R.; Han, L. J.; Xu, B. H.; Zhang, S. J. Highly Efficient Electrocatalytic CO_2 Reduction to C_{2+} Products on a Poly(ionic liquid)-Based Cu^0-Cu^I Tandem Catalyst. *Angew. Chem., Int. Ed.* **2022**, *61* (9), No. e202110657.
(63) Le, J. B.; Fan, Q. Y.; Li, J. Q.; Cheng, J. Molecular origin of negative component of Helmholtz capacitance at electrified Pt(111)/water interface. *Sci. Adv.* **2020**, *6* (41), No. eabb1219.
(64) Li, J.; Xiong, H.; Liu, X.; Wu, D.; Su, D.; Xu, B.; Lu, Q. Weak CO binding sites induced by Cu-Ag interfaces promote CO electroreduction to multi-carbon liquid products. *Nat. Commun.* **2023**, *14* (1), 698.
(65) Schreier, M.; Yoon, Y.; Jackson, M. N.; Surendranath, Y. Competition between H and CO for Active Sites Governs Copper-Mediated Electrosynthesis of Hydrocarbon Fuels. *Angew. Chem., Int. Ed.* **2018**, *57* (32), 10221−10225.
(66) Xiao, H.; Cheng, T.; Goddard, W. A., 3rd Atomistic Mechanisms Underlying Selectivities in C_1 and C_2 Products from Electrochemical Reduction of CO on Cu(111). *J. Am. Chem. Soc.* **2017**, *139* (1), 130−136.
(67) Xiao, H.; Cheng, T.; Goddard, W. A., 3rd; Sundararaman, R. Mechanistic Explanation of the pH Dependence and Onset Potentials for Hydrocarbon Products from Electrochemical Reduction of CO on Cu (111). *J. Am. Chem. Soc.* **2016**, *138* (2), 483−486.
(68) Lu, X.; Shinagawa, T.; Takanabe, K. Product Distribution Control Guided by a Microkinetic Analysis for CO Reduction at High-Flux Electrocatalysis Using Gas-Diffusion Cu Electrodes. *ACS Catal.* **2023**, *13* (3), 1791−1803.
(69) Shen, H.; Wang, Y.; Chakraborty, T.; Zhou, G.; Wang, C.; Fu, X.; Wang, Y.; Zhang, J.; Li, C.; Xu, F.; et al. Asymmetrical C−C Coupling for Electroreduction of CO on Bimetallic Cu−Pd Catalysts. *ACS Catal.* **2022**, *12*, 5275−5283.
(70) Wang, Y.; Li, B.; Xue, B.; Libretto, N.; Xie, Z.; Shen, H.; Wang, C.; Raciti, D.; Marinkovic, N.; Zong, H.; et al. CO electroreduction on single-atom copper. *Sci. Adv.* **2023**, *9* (30), No. eade3557.
(71) Hori, Y.; Koga, O.; Yamazaki, H.; Matsuo, T. Infrared spectroscopy of adsorbed CO and intermediate species in electrochemical reduction of CO_2 to hydrocarbons on a Cu electrode. *Electrochim. Acta* **1995**, *40* (16), 2617−2622.
(72) Wuttig, A.; Liu, C.; Peng, Q.; Yaguchi, M.; Hendon, C. H.; Motobayashi, K.; Ye, S.; Osawa, M.; Surendranath, Y. Tracking a Common Surface-Bound Intermediate during CO_2-to-Fuels Catalysis. *ACS Cent. Sci.* **2016**, *2* (8), 522−528.
(73) Li, J.; Li, C.; Hou, J.; Gao, W.; Chang, X.; Lu, Q.; Xu, B. Intercepting Elusive Intermediates in Cu-Mediated CO Electrochemical Reduction with Alkyl Species. *J. Am. Chem. Soc.* **2022**, *144* (44), 20495−20506.
(74) Li, C. W.; Kanan, M. W. CO_2 reduction at low overpotential on Cu electrodes resulting from the reduction of thick Cu_2O films. *J. Am. Chem. Soc.* **2012**, *134* (17), 7231−7234.
(75) Verdaguer-Casadevall, A.; Li, C. W.; Johansson, T. P.; Scott, S. B.; McKeown, J. T.; Kumar, M.; Stephens, I. E.; Kanan, M. W.; Chorkendorff, I. Probing the Active Surface Sites for CO Reduction on Oxide-Derived Copper Electrocatalysts. *J. Am. Chem. Soc.* **2015**, *137* (31), 9808−9811.
(76) Handoko, A. D.; Ong, C. W.; Huang, Y.; Lee, Z. G.; Lin, L.; Panetti, G. B.; Yeo, B. S. Mechanistic Insights into the Selective Electroreduction of Carbon Dioxide to Ethylene on Cu_2O-Derived Copper Catalysts. *J. Phys. Chem. C* **2016**, *120* (36), 20058−20067.
(77) Eilert, A.; Cavalca, F.; Roberts, F. S.; Osterwalder, J.; Liu, C.; Favaro, M.; Crumlin, E. J.; Ogasawara, H.; Friebel, D.; Pettersson, L. G.; et al. Subsurface Oxygen in Oxide-Derived Copper Electrocatalysts for Carbon Dioxide Reduction. *J. Phys. Chem. Lett.* **2017**, *8* (1), 285−290.
(78) Li, F.; Thevenon, A.; Rosas-Hernandez, A.; Wang, Z.; Li, Y.; Gabardo, C. M.; Ozden, A.; Dinh, C. T.; Li, J.; Wang, Y.; et al. Molecular tuning of CO_2-to-ethylene conversion. *Nature* **2020**, *577* (7791), 509−513.
(79) Zhao, S.; Christensen, O.; Sun, Z.; Liang, H.; Bagger, A.; Torbensen, K.; Nazari, P.; Lauritsen, J. V.; Pedersen, S. U.; Rossmeisl, J.; et al. Steering carbon dioxide reduction toward C-C coupling using copper electrodes modified with porous molecular films. *Nat. Commun.* **2023**, *14* (1), 844.
(80) Chen, P.; Wu, Y.; Rufford, T. E.; Wang, L.; Wang, G.; Wang, Z. Organic molecules involved in Cu-based electrocatalysts for selective CO_2 reduction to C_{2+} products. *Materials Today Chemistry* **2023**, *27*, 101328.
(81) Ma, S.; Sadakiyo, M.; Heima, M.; Luo, R.; Haasch, R. T.; Gold, J. I.; Yamauchi, M.; Kenis, P. J. Electroreduction of Carbon Dioxide to Hydrocarbons Using Bimetallic Cu-Pd Catalysts with Different Mixing Patterns. *J. Am. Chem. Soc.* **2017**, *139* (1), 47−50.
(82) Ji, Y.; Chen, Z.; Wei, R.; Yang, C.; Wang, Y.; Xu, J.; Zhang, H.; Guan, A.; Chen, J.; Sham, T.-K.; et al. Selective CO-to-acetate electroreduction via intermediate adsorption tuning on ordered Cu−Pd sites. *Nat. Catal.* **2022**, *5* (4), 251−258.
(83) Xie, M.; Shen, Y.; Ma, W.; Wei, D.; Zhang, B.; Wang, Z.; Wang, Y.; Zhang, Q.; Xie, S.; Wang, C.; et al. Fast Screening for Copper-Based Bimetallic Electrocatalysts: Efficient Electrocatalytic Reduction of CO_2 to C_{2+} Products on Magnesium-Modified Copper. *Angew. Chem., Int. Ed.* **2022**, *61* (51), No. e202213423.
(84) Schouten, K. J. P.; Kwon, Y.; van der Ham, C. J. M.; Qin, Z.; Koper, M. T. M. A new mechanism for the selectivity to C_1 and C_2 species in the electrochemical reduction of carbon dioxide on copper electrodes. *Chem. Sci.* **2011**, *2* (10), 1902−1909.
(85) Clark, E. L.; Bell, A. T. Direct Observation of the Local Reaction Environment during the Electrochemical Reduction of CO_2. *J. Am. Chem. Soc.* **2018**, *140* (22), 7012−7020.
(86) Ledezma-Yanez, I.; Gallent, E. P.; Koper, M. T. M.; Calle-Vallejo, F. Structure-sensitive electroreduction of acetaldehyde to ethanol on copper and its mechanistic implications for CO and CO_2 reduction. *Catal. Today* **2016**, *262*, 90−94.
(87) Xu, B.; Madix, R. J.; Friend, C. M. Activated metallic gold as an agent for direct methoxycarbonylation. *J. Am. Chem. Soc.* **2011**, *133* (50), 20378−20383.
(88) da Silva, A. H. M.; Lenne, Q.; Vos, R. E.; Koper, M. T. M. Competition of CO and Acetaldehyde Adsorption and Reduction on Copper Electrodes and Its Impact on n-Propanol Formation. *ACS Catal.* **2023**, *13* (7), 4339−4347.
(89) Chen, C.; Yu, S.; Yang, Y.; Louisia, S.; Roh, I.; Jin, J.; Chen, S.; Chen, P.-C.; Shan, Y.; Yang, P. Exploration of the bio-analogous asymmetric C−C coupling mechanism in tandem CO_2 electroreduction. *Nat. Catal.* **2022**, *5* (10), 878−887.
(90) Wang, X.; de Araujo, J. F.; Ju, W.; Bagger, A.; Schmies, H.; Kuhl, S.; Rossmeisl, J.; Strasser, P. Mechanistic reaction pathways of enhanced ethylene yields during electroreduction of CO_2-CO co-feeds on Cu and Cu-tandem electrocatalysts. *Nat. Nanotechnol* **2019**, *14* (11), 1063−1070.
(91) Lum, Y.; Ager, J. W. Evidence for product-specific active sites on oxide-derived Cu catalysts for electrochemical CO_2 reduction. *Nat. Catal.* **2019**, *2* (1), 86−93.
(92) Ling, N.; Zhang, J.; Wang, M.; Wang, Z.; Mi, Z.; Bin Dolmanan, S.; Zhang, M.; Wang, B.; Ru Leow, W.; Zhang, J.; et al. Acidic Media Impedes Tandem Catalysis Reaction Pathways in Electrochemical CO_2 Reduction. *Angew. Chem., Int. Ed.* **2023**, *62*, No. e202308782.
(93) Gao, W.; Xu, Y.; Fu, L.; Chang, X.; Xu, B. Experimental evidence of distinct sites for CO_2-to-CO and CO conversion on Cu in

https://doi.org/10.1021/jacsau.3c00494
JACS Au 2023, 3, 2948−2963

the electrochemical CO_2 reduction reaction. *Nat. Catal.* **2023**, DOI: 10.1038/s41929-023-01002-6.

(94) Wei, P.; Gao, D.; Liu, T.; Li, H.; Sang, J.; Wang, C.; Cai, R.; Wang, G.; Bao, X. Coverage-driven selectivity switch from ethylene to acetate in high-rate CO_2/CO electrolysis. *Nat. Nanotechnol* **2023**, *18* (3), 299−306.

https://doi.org/10.1021/jacsau.3c00494
JACS Au 2023, 3, 2948−2963